NASA Contractor Report 159171

Gyrodampers for Large Space Structures

LOCKHEED PALO ALTO RESEARCH LABORATORY
Palo Alto, CA 94304

CONTRACT NAS1-14887-TASK 6
FEBRUARY 1979

National Aeronautics and
Space Administration

Langley Research Center
Hampton, Virginia 23665
AC 804 827-3966

NASA Contractor Report 159171

Gyrodampers for Large Space Structures

J. N. Aubrun and
G. Margulies

LOCKHEED PALO ALTO RESEARCH LABORATORY
Palo Alto, CA 94304

CONTRACT NAS1-14887-TASK 6
FEBRUARY 1979

National Aeronautics and
Space Administration

Langley Research Center
Hampton, Virginia 23665
AC 804 827-3966

TABLE OF CONTENTS

ILLUSTRATIONS

TABLES

SUMMARY

This report addresses the problem of controlling the vibrations of large space structures by the use of actively augmented damping devices distributed throughout the structure.

When these devices introduce only a moderate amount of damping (10% - 20%), simple analytical formulas are obtained for either predicting the damping or designing the dampers from the application of the theory of Low Authority Controllers to structural control. Such control systems are shown to be always stable and not very sensitive to parameter changes or uncertainties when actuator and sensor are colocated, i.e., each damping device is a self-contained unit attached to the structure and acting as an energy sink.

A newly conceived damping device, the gyrodamper, is described and analyzed. It consists of a set of single gimbal control moment gyros which are actively controlled to extract the structural vibratory energy through the local rotational deformations of the structure. Various linear and nonlinear dynamic simulations of gyrodamped beams are shown, including results on self-induced vibrations due to sensor noise and rotor imbalance. The complete nonlinear dynamic equations are shown in Appendix A.

The problem of designing and sizing a system of gyrodampers for a given structure, or extrapolating results for one gyrodamped structure to another is solved in terms of scaling laws. Novel scaling laws for gyro systems are derived, based upon fundamental physical principles, and various examples are given.

INTRODUCTION AND OVERVIEW

In the development of large structures constructed or assembled in space, it is of interest to determine the effectivenss of active devices which augment structural damping. Natural damping in large structures can be significantly enhanced by incorporating into the structure energy dissipation devices which transform the vibratory motions into heat, either directly by mechanical friction (e.g., passive dashpots) or through electrical networks (e.g., active electrodynamic actuators). In the latter case, a sensing device is required to measure the structural vibration velocities which are fed back to the actuator with the proper gain so that the colocated sensor/actuator will mimic a purely passive device. Such active damping devices (sometimes called augmented passive dampers) differ essentially from purely passive devices because they are effective over a broad range of structural vibration frequencies, whereas a passive device can only be tuned effectively for a single frequency.

In general, the sensitivity of energy absorption characteristics of augmented passive dampers is far superior to what can be achieved by purely passive means such as mechanical friction. The advantages of augmented dampers include also their adaptability and reliability characteristics, primarily because electrical devices fare better in the harsh space environment than do viscous fluids or materials whose granular friction characteristics must remain constant, or at least predictable.

Structural dampers can be classified to reflect the duality between translation/force and rotation/torque, as well as the criterion which distinguishes where the reaction forces or torques are transmitted. If these reactions are transmitted back into the structure,the dampers are intrastructural, while if they are transmitted to inertial space, the dampers are inertial. The corresponding classification matrix, with some generic examples, is shown below, with additional detail shown in Fig. 4 of the report.

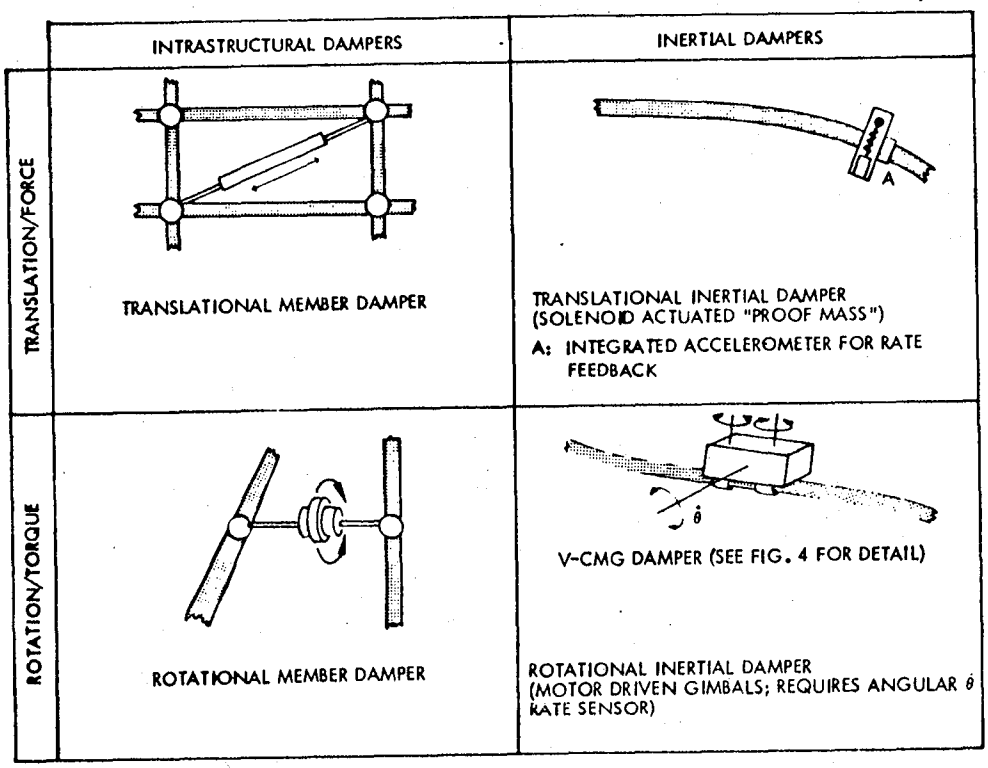

Classification Matrix of Damping Devices and Generic Examples

In the present study, attention is focused on a class of inertial torque-producing devices called gyrodampers. In their simplest form, the so-called V-CMG damper illustrated in Fig. 4 of this report, a pair of identical control moment gyros (CMGs) are mounted "back-to-back" on parallel gimbal axes so that, in this nominal position, their angular momenta are equal and opposite and hence cancel. Gimbal motion commands are also equal and opposite, resulting in symmetric V-scissoring motions of the CMG angular momentum vectors about a fixed axis. Thus, the resulting torque (vector sum of the individual rates-of-change of angular momentum) always lies along this axis. This torque, applied to the structure by the gyros, is then electronically controlled so as to mimic the effect of an (inertial) rotational dashpot opposing the rate-of-change of local structural angular rotation.

A purely passive version of the V-CMG dampers were developed at Lockheed in 1963 for gravity-gradient attitude stabilization of the Agena vehicle and were subsequently flight-tested several times – very successfully. At that time, the V-CMG dampers were constructed from oversized rate-sensing gyros used in a reversed role, i.e., that of actuators producing inertial rigid-body damping torques rather than sensors measuring rotational rates; see Refs. 11 and 12.

The genesis of the gyrodamper can be understood most easily by examining intuitively the basic properties of the simplest inertial damper, the so-called proof-mass damper depicted above in the upper right-hand corner of the damper classification matrix. If we consider a generic flexible space structure as an oscillating spatial sinusoid, it is clear that the "optimum" location for a proof-mass damper is the anti-nodal point where translational velocities are maximum; these velocities are measured by the damper's (colocated) sensor and fed back to an electronic control system which drives the proof-mass so as to mimic the effect of an inertial dashpot. As this damper is relocated closer to the nodal point, its effectiveness diminishes in that a higher feedback gain (i.e., higher damping force) is required where there is less structural motion. In the limit, the proof-mass damper is totally ineffective when located at the nodal point where there is no structural motion.

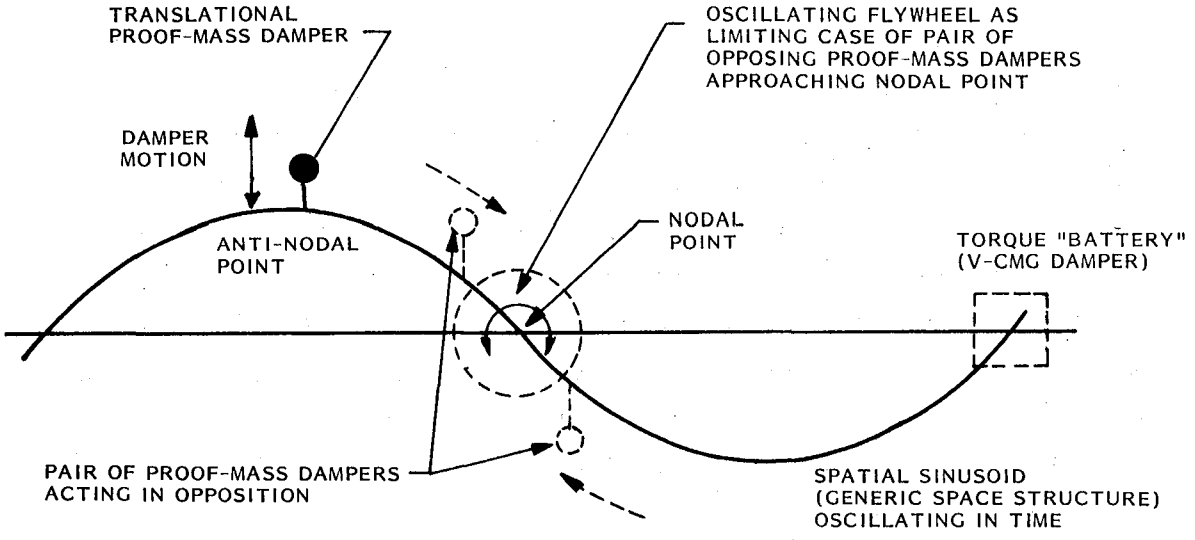

Proof-Mass Dampers, Flywheel and V-CMG Gyrodampers

When two proof-mass dampers are considered, symmetrically situated about a nodal point and acting in opposition (see diagram) they produce a damping force couple about the nodal point. In the limit, as they approach the nodal point, they can be replaced conceptually by an oscillating flywheel pivoted at the nodal point. The inertial "flywheel damper" represents thus the limiting case of a pair of very inefficiently located opposing proof-mass dampers. Indeed, not only are high torque levels required, but also high wheel inertia, with a corresponding high weight penalty. The flywheel damper does not appear thus as a very efficient device to produce inertial reaction torques about nodal points. However, it has an advantage at very low frequencies in that it is only velocity-limited whereas the proof-mass is displacement-limited.

By contrast, the gyrodamper (located also at nodal points) can be considered as a "black box" torque battery, capable of producing high inertial torques without requiring the counter-rotation of large inertias. The essential characteristic of gyrodampers is their angular momentum storage capability. Because it is not possible to store linear momentum, there is no translational analogue to the gyrodamper, which must therefore be regarded as a unique device for producing inertial torques for structural damping.

A general property of intertial dampers is their inability to transmit structural vibration energy from one part of the structure to another, as can occur when several intrastructural member dampers are used simultaneously (Ref. 5). By contrast, the simultaneous use of several inertial dampers is "decoupled" in the sense that each one provides an independent inertial energy sink. Nevertheless, non-inertial dampers (other than member dampers) may be required for very low frequencies or global reshaping (e.g., curvature control), rather than just for vibration suppression. A heuristic chart, showing the range of operation of various types of actuators is shown below.

In this chart, potential prototype actuators are sketched roughly in the middle of their bandwidth (horizontal scale), and at the bottom of their vibration suppression range (vertical scale). The devices shown do not yet exist as vibration control devices for space structures, and their characteristics overlap quite

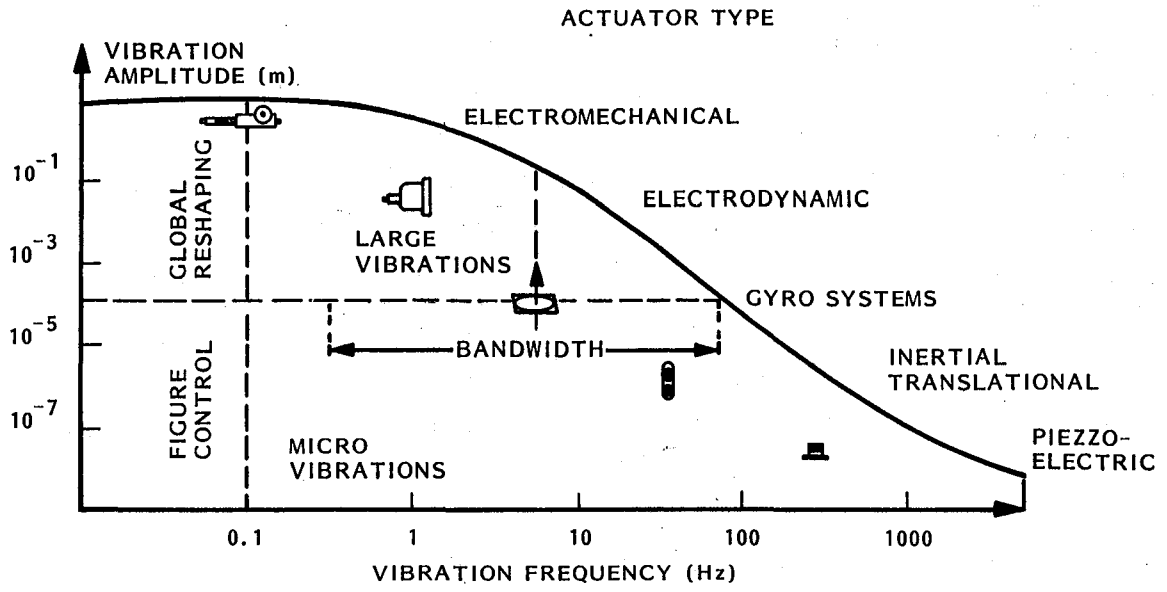

Range of Operation of Various Actuator Types

significantly. This study focuses on gyrodampers because of their central range of operation and their potentially remarkable performance as high-torque level inertial rotational dampers. The principal drawback of gyrodampers, at the present time, is due to the nature of their principal component devices, the control moment gyros (CMGs). These are not off-the-shelf components, but rather custom-built, "few-of-a-kind" devices whose exorbitant cost includes the associated R&D development work. (Appendix C illustrates this point for a particular manufacturer who lists six CMG models, for a total of 30 units built.)

The first section of the present study addresses structural vibrations which can be controlled by distributed systems of sensors and actuators with limited damping authority, i.e., the control system is allowed to modify only moderately the natural modes and frequencies of the structure. This is typically the case when the usually low natural damping of a structure is augmented by passive or active dampers to produce 10 - 20% damping in the principal modes. While it is relatively easy to model such devices and analyze the characteristics of the total system, an a priori prediction of their effect is not feasible because no analytical

expression exists for the roots of high-order polynomials and for eigenvectors of large matrices. Thus any modification of the original structure, as occurs for instance when damping devices are embedded in it, will lead to a new set of complex eigenvalues/eigenvectors that need to be determined all over again by numerical processes. This a posteriori evaluation is quite cumbersome, and the original design decision on locating and sizing the dampers is then essentially based on guess work and engineering judgment.

A novel idea presented in this study is that it is possible to apply root perturbation techniques to predict analytically the behavior of the total system. A new formula is established for the eigenvector perturbation which helps define the validity range of the well-known Jacobi root perturbation formula. Analytical formulas are then derived relating the root shifts and mode shape changes to the controllers' gains, and these can be used both for performance prediction and controller design. These topics are the principal elements of J. N. Auburn's Low Authority Structurual Control Theory (Ref. 1), and are presented in the first section of the report.

The remaining sections of the report address the basic physical principles, dynamics, operational characteristics and scaling laws of gyrodampers. These actuators were studied primarily in the context of planar beam vibrations, using a 100-m GrEp beam as a preliminary design, but the extension of the concept to beam-like space platforms became readily apparent and is addressed in the last section dealing with Scaling Laws. Appendix A, prepared by D. A. Levinson, outlines the derivation of the equations of planar motion of a free-free beam equipped with an arbitrary number of single-axis V-gyrodampers, arbitrarily located on the beam. These equations include the nonlinear actuator dynamics of the gyros, and are, conceptually, a special case of more general equations of three-dimensional motion of an arbitrary finite-element free-free structure equipped with arbitrarily many gyros. (The associated computer program GDS, Gyrodamped Structures, is a modular "N-Body" program being developed under the Lockheed Independent Research Program.)

Appendix B on Local Rotation Modes presents a derivation of the nth modal rotation coefficients, i.e., the contributions of the nth mode of a structure to the local instantaneous axis of rotation at a point. It is shown, based on an 1858 theorem due to Helmholtz, that this local rotation axis is obtained as a linear modal combination of the curls of the individual modal deformation vector-fields. Finally, Appendix C illustrates the gyrodamper scaling process for a 340 lb, 23' free-free aluminum beam whose planar oscillations are to be damped by one-axis V-CMG systems mounted at its free ends.

LIST OF SYMBOLS*

a	subscript relative to an actuator
A	dynamic matrix of a linear system (square matrix)
A'	dynamic matrix modified by the control system
B	damping matrix (also denotes beam, with no ambiguity in context)
B_{mn}	element of matrix B
$C_1, C_2, \ldots, C_6$	scaling constants
d	column matrix containing nonzero D_{ar} elements (also gyrodamper damping gain, with no ambiguity in context)
D	matrix of damping gains (or scalar for one damper only)
D_{ar}	element of matrix D
$\{\vec{e}_1, \vec{e}_2, \vec{e}_3\}$	orthonormal frame locally attached to beam
E	Young's modulus
$f_a(t)$	input to a distributed force actuator a
f_{aj}	load applied at nodal station j by distributed actuator a
F	column matrix of applied forces
F_a	elements of F
G_n	weighting matrix
$\vec{h}, h$	angular momentum (and its magnitude) carried by one gyro
$\vec{h}_1, \vec{h}_2, \ldots$	angular momentum vectors of gyro 1, 2, ...
H	distributed sensor matrix
$\vec{H}$	total angular momentum of gyro mounted on vibrating beam B
i	imaginary unit ($i^2 = -1$)

*Excluding Appendix A which is self-contained; all symbols are defined therein, and because it involves derivation of equations, are much too numerous to be listed separately.

I	identity matrix, identity dyadic sectional inertia of a beam total beam + gyro inertia (no ambiguity in context)
j	subscript relative to a nodal station
J	total inertia of a gyro about its gimbal axis
J_s	spin inertia of gyro rotor
k	spring constant (proportional gain)
K	gyro rate-feedback gain
K'	normalized gain = $(K + h)/J$
K_G	gimbal torque gyro scaling parameter
K_H	momentum gyro scaling parameter
K_J	gimbal inertia gyro scaling parameter
K_{J_s}	spin inertia gyro scaling parameter
K_P	dissipated power gyro scaling parameter
K_R	rotor strength gyro scaling parameter
K_S	bending stiffness structural scaling parameter
ℓ	characteristic length of idealized gyro rotor radius
L	beam length
L_n	nth left eigenvector of matrix A
m	mass of a V-gyrodamper unit subscript relative to mth mode (no ambiguity in context)
n	subscript relative to the nth mode
M	mass matrix of finite-element structural modal total structural mass (no ambiguity in context)
N	number of V-gyrodamper units
N_a	number of actuators
N_c	number of modes to be controlled
N_d	number of nonzero gains D_{ar}
N_m	number of modes
N_r	number of sensors
N_s	number of nodal stations

P	distributed actuator matrix
P_p	peak dissipated power by gyro gimbal torque motor
q	vector of modal amplitude, N_m components
r	subscript relative to a sensor
R_n	nth right eigenvector of matrix A
R_E	electrical resistance of one winding turn
s	Laplace transform variable
S	matrix relating damping gains to damping ratios
S_{ni}	element of matrix S; $S_{ni} = \phi_{a_i n}\, \phi_{r_i n}$ (see below)
$\mathcal{S}$	strain tensor
t	time
$\vec{T}_g$, T_g	external "passive" torque, magnitude, applied to gyro by gimbal motor
T_G	total "active" torque applied to the gyro gimbal, $= (h + K)\dot{\theta} + T_g$
T_V	"vehicle" torque applied by gyro system to the structure
$T(q)$	linear combination of system "modal torques"
u	column matrix of structural deformations (N_s components)
$\vec{u}_i$	physical vector of deformation at nodal station i (3 components)
$\vec{u}(\vec{r}, t)$	physical time-varying vector field of deformation at point $\vec{r}$, time t
x	abscissa of a point on the beam
y	column matrix of distributed sensor outputs
y_r	components of y
z	complex column vector
β_n	dimensionless nth root of frequency equation for a free-free beam
σ	gyro gimbal angle
ω	vibration cyclic frequency (rad/s)
ω_n	nth mode cyclic frequency (rad/s)
ω_1	upper limit of gyrodamper bandwidth
ω_G^2	$\equiv k/J$
ω_o	lower limit ($\equiv \omega_G^2/\omega_1$) of gyrodamper bandwidth

ϕ_{jn}	amplitude of nth mode shape at nodal station j
Φ	matrix of mode shapes
Φ^R, Φ^A	matrices of generalized mode shapes
ψ_n	nth complex mode shape
ζ	damping ratio
ζ_n	damping ratio of nth mode
θ	inertial angular rotation of a structural neighborhood about one axis
$\vec{\delta\theta}$	instantaneous axis of rotation corresponding to deformation field $\vec{u}(\vec{r}, t)$
$\vec{\delta\theta}_n$	nth "modal rotation coefficient" (physical vector, 3 components)
$\vec{\Omega}_B$	inertial angular velocity of the beam + gyro system
Ω_s	spin rate of the gyro rotor

LOW AUTHORITY STRUCTURAL CONTROL THEORY

This theory addresses the analytical prediction of the behavior of structures controlled by distributed systems of sensors and actuators with limited authority, i.e., the control system is allowed to modify only moderately the natural modes and frequencies of the structure. This is typically the case when the (usually low) natural damping of a structure is augmented by passive or active devices (so-called dampers). For instance, starting with an undamped structure, and placing dampers in it in such a way that, say, 10% system damping is obtained in the principal modes, implies that the relative change $|d\lambda_n/\lambda_n|$ of the corresponding complex root $\lambda_n = i\omega_n$ is only 10%. This change is small enough to justify first-order expansions, i.e., to warrant the use of root perturbation methods. The following section will outline the basic formulas of the eigensystem perturbation theory.

Jacobi's Formula Revisited and Further Generalizations

The root perturbation formula was first derived by Jacobi (ref. 2) for infinitesimal perturbations which neglect the induced eigenvector perturbation. Formulas for perturbing the eigenvectors are developed here, leading to a more general form of Jacobi's formula.

Consider first a square matrix A and one of its eigenvalues, say λ_n, and the corresponding left and right eigenvectors L_n and R_n defined by:

$$A R_n = \lambda_n R_n \tag{1}$$

$$L_n^T A = \lambda_n L_n^T \tag{2}$$

Assuming now a change δA in the coefficients of the matrix A so that A becomes $A' = A + \delta A$, the quantities λ_n and R_n change correspondingly by $\delta\lambda_n$ and δR_n such that one now obtains

$$(A + \delta A)(R_n + \delta R_n) = (\lambda_n + \delta\lambda_n)(R_n + \delta R_n)$$

which, after substituting (1), reduces to:

$$A\,\delta R_n + \delta A\,(R_n + \delta R_n) = \lambda_n\,\delta R_n + \delta\lambda_n\,(R_n + \delta R_n) \tag{3}$$

Multiplying the matrix equation (3) on the left by L_n^T and using Eq. (2), one obtains the exact formula

$$\delta\lambda_n = \frac{L_n^T\,\delta A\,(R_n + \delta R_n)}{L_n^T\,(R_n + \delta R_n)} \tag{4}$$

Jacobi's formula can now be obtained from (4) by assuming δR_n to be sufficiently small to be ignored and writing "$\delta \rightarrow d$:"

$$d\lambda_n = \frac{L_n^T\,dA\,R_n}{L_n^T\,R_n} \quad \text{(Jacobi)} \tag{5}$$

The perturbation in the eigenvector itself is less obvious to obtain, due to the fact that an eigenvector is only defined within a multiplicative constant. Thus, some normalization must be introduced so that the eigendirection δR_n can be uniquely defined. To accomplish this, another perturbation formula is obtained by multiplying (3) on the left by $R_n^T G$, where G_n is a normalization weighting matrix such that

$$R_n^T G_n R_n = 1$$

Thus, for sufficiently small δR_n, denoted by dR_n, we have

$$R_n^T G_n \, dR_n = 0 \tag{6}$$

(Note: Because R_n is a complex vector, it could be normalized by dividing it by its length $\|R_n\|$ and denoted by $\hat{R}_n$, where $\|$ denotes the usual Hermitian norm. If $(\,,\,)$ denotes then the corresponding Hermitian inner-product, it is generally true, in contradistinction to the real case, that $(\hat{R}_n, d\hat{R}_n) \neq 0$. This motivates the use of the weighting matrix G_n.)

After expanding (3), multiplying on the left by $R_n^T G_n$, and using (6), one obtains

$$d\lambda_n \cong R_n^T G_n \, dA \, R_n + R_n^T G_n A \, dR_n$$

This expression is then used to eliminate $d\lambda_n$ in (3), leading to:

$$dR_n = \left(A - R_n R_n^T G_n A - \lambda_n I\right)^{-1} \left(R_n R_n^T G_n - I\right) dA \, R_n \tag{7}$$

A second-order perturbation may then be obtained for $d\lambda_n$ by using (7) in (4), rewritten with $\delta \to d$ [see Eq. (26)].

State-Space Structural Equations and Modal Eigenvectors

To apply the preceding formulas to the control of a structure, it is necessary to obtain structural equations in first-order form.

In the lumped-mass finite-element appraoch, a structure is modeled by point-masses connected by various structural elements representing stiffnesses. In the consistent-mass finite-element model, rotational as well as translational degrees of freedom may also be taken into account at element nodes. Although

the results presented here are valid for this type of model, implementation of the consistent-mass approach is somewhat more involved and, therefore, only lumped-mass models will be considered, where each mass m_i, at node i, is described by its displacement $\vec{u}_i$. If N_s nodes are involved in the model, the total system has $3N_s$ degrees of freedom. The dynamic equations of the structure, which are linear for small displacements, may be written as:

$$M\ddot{u} + Ku = F \tag{8}$$

where u is a column vector obtained by stacking the components of the N_s vectors $\vec{u}_i$, F is obtained in the same way from the local loads $\vec{F}_i$, and M and K are $N_m \times N_m$ matrices ($N_m = 3N_s$).

The usual procedure is then to diagonalize (8) by solving the eigenproblem:

$$M^{-1} K \Phi = \Phi \left[\omega_n^2\right]$$

where Φ is a matrix of eigenvectors or <u>mode shapes</u> and $\omega_n/2\pi$ is the frequency associated with mode n. Because of reciprocity properties, K and M are symmetric matrices (M is diagnonal), and it is known (Ref. 3) that there exist a normalization of Φ such that:

$$\Phi^T M \Phi = I \quad \text{(I: identity matrix)}$$

and thus

$$\Phi^T K \Phi = \left[\omega_n^2\right]$$

(Note that the elements of Φ have the dimension of the reciprocal square root of mass.)

By defining the transformation:

$$u = \Phi q \tag{9}$$

where q is a vector of modal amplitudes, Eq. (8) may be transformed into the classical modal equations

$$\ddot{q} + \begin{bmatrix} \ddots & \\ & \omega_n^2 \\ & & \ddots \end{bmatrix} q = \Phi^T F$$

By defining the state-vector:

$$X \equiv \begin{bmatrix} \dot{q} \\ \\ q \end{bmatrix}$$

the modal equation is finally written in first-order form as:

$$\dot{X} = AX + \begin{bmatrix} \Phi^T \\ \\ 0 \end{bmatrix} F \tag{10}$$

where

$$A \equiv \left[\begin{array}{c|c} 0 & \begin{matrix} \ddots & \\ & -\omega_n^2 \\ & & \ddots \end{matrix} \\ \hline I & 0 \end{array}\right]$$

Complex eigenvalues and eigenvectors are now associated with the matrix A. [Note: the eigenvectors of A (in the usual sense) are called the right eigenvectors of A because the eigenproblem is written as $AR_n = \lambda_n R_n$. The eigenvectors of

A^T (in the usual sense) are called the left eigenvectors of A because the eigenproblem $A^T L_n = \lambda_n L_n$ can also be written $L_n^T A = \lambda_n L_n^T$. These two types of eigenvectors eliminate the simultaneous use of A and A^T.]

The eigenvalues of A are $\lambda_n = \pm i\omega_n$ ($i^2 = -1$, and $n = 1, 2, \ldots N_m$) and the modal state eigenvectors are defined to be the right and left eigenvectors of A corresponding to $\lambda_n = +i\omega_n$, i.e.,

$$R_n \equiv \left[0 \quad 0\ldots0 \; i\omega_n \; 0\ldots0 \;\middle|\; 0 \quad 0\ldots0 \quad 1 \quad 0\ldots0\right]^T$$
$$L_n \equiv \left[0 \quad 0\ldots0 \quad 1 \quad 0\ldots0 \;\middle|\; 0 \quad 0\ldots0 \; i\omega_n \; 0\ldots0\right]^T \tag{11}$$

where the only nonzero elements occur in position n and $n + N_m$.

Fundamental Modal Damping Prediction Formula

Damping may be introduced in the structure by measuring (components of) velocities* $\dot{u}_r$ at some sensor location r ($r = 1, 2, \ldots, N_r$) and producing forces F_a at actuator locations a ($a = 1, 2, \ldots N_a$) such that, in general

$$F_a = -\sum_r D_{ar} \dot{u}_r \tag{12}$$

where the D_{ar}'s are positive damping (rate-feedback) gains, collectively denoted by the matrix D which is augmented by zeros to be dimensionally compatible with the

*It should be noted again that F_j really denotes one component of the load at some node and u_i one component of the deformation at the same or at another node. For instance F_8 may denote the y-component of a force actuator at some node, while F_9 is the z-component at the same node.

modal matrix Φ, so that Eq. (12) can be written as $F = -D\dot{u}$, which is also equal to $-D\Phi\dot{q}$ according to (9). Thus the structural Eq. (10) becomes:

$$\dot{X} = A'X \tag{13}$$

where

$$A' = A + dA \equiv \left[\begin{array}{c|c} -\Phi^T D\Phi & \ddots\ \omega_n^2 \\ \hline I & 0 \end{array}\right]$$

The new roots of the linear system (13) may then be obtained by considering the matrix

$$dA \equiv \left[\begin{array}{c|c} -\Phi^T D\Phi & 0 \\ \hline 0 & 0 \end{array}\right] \tag{14}$$

as a perturbation of the original matrix A and applying the formulas of Section 1.1.

To the original (undamped) mode of frequency $\omega_n/2\pi$ corresponds the eigenvalue $\lambda_n = i\omega_n$. If the state-space matrix A is now perturbed by dA by the introduction of "moderate" damping (rate-feedback) according to (14), the original mode will now have the eigenvalue $\lambda_n + d\lambda_n$, where $d\lambda_n$ is given by Jacobi's formula (5).

From (11) we have

$$L_n^T R_n = 2i\omega_n$$

For brevity, define the matrix $B = [B_{kn}]$ and the vector $Z = \left[Z_1, Z_2, \ldots Z_{2N_m}\right]^T$ by:

$$\left.\begin{aligned} B &\equiv \Phi^T D\Phi \\ Z &\equiv dA\, R_n \end{aligned}\right\} \tag{15}$$

Then from (11) and (14) we obtain:

$$Z_k = \begin{cases} -i\omega_n B_{kn} & \text{for} \quad k = 1, 2, \ldots, N_m \\ 0 & \text{for} \quad k > N_m \end{cases}$$

and thus

$$L_n^T Z = -i B_{nn} \omega_n$$

Consequently, Jacobi's formula leads to

$$d\lambda_n \cong -\frac{1}{2} B_{nn} = -\frac{1}{2} \sum_{a,r} D_{ar} \phi_{an} \phi_{rn}$$

where ϕ_{an}, ϕ_{rn} are the elements of the modal matrix Φ corresponding to the nth mode, at actuator nodal stations a and sensor nodal stations r. Since the ϕ's and D's (positive rate-feedback gains) are real, it follows that the new root $\lambda_n + d\lambda_n$ has now a real part, and with the usual interpretation of damping ratio we obtain the fundamental modal damping prediction formula:

$$\boxed{2 \zeta_n \omega_n \cong \sum_{a,r} D_{ar} \phi_{an} \phi_{rn}} \qquad (16)$$

This is thus a general formula for predicting modal damping in a rate-feedback system of distributed sensors ($r = 1, 2, \ldots, N_r$) and actuators ($a = 1, 2, \ldots, N_a$). It confirms the intuitive idea that sensors and actuators should be located preferably where large modal deflections occur, i.e., where mode shapes have large magnitude. Obviously, if ϕ_{rn} is zero, mode #n is not observable and if ϕ_{an} is zero, it is not

controllable. Moreover, formula (16) gives quantitative estimates of modal damping and stability. A very significant consequence of (16) is that when $a = r$, i.e., when sensors and actuators are colocated, the structure is always stable since, for positive D's , the sum on the right-hand side is always positive for any n .

Damper Design and System Robustness

It is now possible to address the main topic of this project which is the design of a control system for damping the structure. Assuming that certain locations have been selected for actuators and sensors, the problem is to determine the gains D_{ar} which will result in desired damping ratios ζ_n . First, the symmetry of Eq. (16) indicates that actuator a and sensor r can be exchanged without changing the value of ζ . Thus, it is only necessary to define the D_{ar}'s for, say $a \geq r$. Next, some D_{ar}'s may be constrained to be zero a priori; i.e., no feedback is intended from sensor r to actuator a . Thus a vector d containing all the nonzero D_{ar}'s is constructed, each component d_i corresponding to a particular $D_{a_i r_i}$.

By defining the matrix S of elements $S_{ni} = \phi_{a_i n} \phi_{r_i n}$, Eq. (16) may be rewritten as

$$(\zeta\omega) = Sd \tag{17}$$

where $(\zeta\omega)$ is the vector of components $\zeta_n \omega_n$ $(n = 1, \ldots N_c)$. If d contains N_d components, the matrix S is then $N_c \times N_d$. In general it will be possible to choose a priori the damping ratios of N_c modes if $N_d = N_c$, by inverting (17):

$$d = S^{-1} (\zeta\omega) \tag{18}$$

If $N_c \neq N_d$ other methods must be used involving pseudo-inverses, linear programming, or other optimization schemes, and this is a wide open field for investigation. In the case of colocated sensor/actuator damping units, N_d is simply equal to the number of damping units, and thus the following result: in order to impose a damping ratio to N_c structural modes, N_c damping units are required.

Imposing a priori damping ratios on the system modes of the damper-augmented system is not necessarily the best design procedure. As a matter of fact, preliminary computer simulations have shown that this approach will almost invariably lead to the use of "negative dampers" (some of the D_{aa}'s turn out to be negative); i.e., some of these devices have to put energy into the structure in order to achieve the desired damping ratios. Since such "negative gain" devices are inherently unstable (even though the truncated system is stable), it is quite certain that the actual system with all its modes will be destabilized. Thus it is necessary to constrain the D_{ar}'s by some of the aforementioned methods used when N_c is different from N_d.

This observation brings about the question of the sensitivity of the damping system to structural parameter changes and uncertainties, or conversely, the so-called "robustness" of this system. Assuming that the nth structural mode shape is only known within a relative error denoted by $\delta\phi_n/\phi_n$, the corresponding relative error on ζ_n may be obtained from Eq. (16) and is given by:

$$\frac{\delta(\zeta_n \omega_n)}{\zeta_n \omega_n} \leq 2 \frac{\sum_{a,r} \left| D_{ar} \phi_{an} \phi_{rn} \right|}{\sum_{a,r} D_{ar} \phi_{an} \phi_{rn}} \cdot \frac{\delta\phi_n}{\phi_n} \tag{19}$$

In general, the sum in the numerator of (19) will be larger than the sum in the denominator, and a small error in the mode shapes may induce enough change in the ζ's so as to drive the system unstable. However, when actuators and sensors are colocated, i.e., when D_{ar} is zero if $a \neq r$, the sensitivity is minimum and (18) becomes:

$$\frac{\delta(\zeta_n \omega_n)}{\zeta_n \omega_n} \leq 2 \frac{\delta\phi_n}{\phi_n} \tag{20}$$

Complex Mode Shapes and Second-Order Formulas

While in the undamped structure the mode shapes are real, i.e., all the points of the structure move in synchrony, this ceases to be true in general when active control is introduced. Instead, the closed-loop mode shapes are characterized by the

fact that there are phase shifts associated with each point of the structure. Thus the new mode shape may be decomposed in an in-phase part (real part) and a 90° out-of-phase part (imaginary part)

$$\psi_n = \psi_n^R + i\,\psi_n^I \tag{21}$$

Since $u = \Phi q$, ψ_n is the value of u when q is equal to the nth eigensolution of the closed-loop equation (13) which is simply $\left(R_n^o + \delta R_n^o\right)$ where R_n^o is a partition of R_n containing the last N_m components of R_n :

$$R_n = \left[R_n' \;\vdots\; R_n^o \right]^T$$

Thus

$$\psi_n = \phi_n + \Phi\,\delta R_n^o \tag{22}$$

An approximate expression for the vector δR_n^o may be calculated explicitly using Eq. (7) in which the matrix G_n is chosen of the form

$$G_n = \begin{bmatrix} 0 & & 0 \\ & \frac{1}{2\omega_n^2} & \\ 0 & & \frac{1}{2} \\ & & 0 \end{bmatrix} \begin{matrix} \\ \leftarrow \text{row n} \\ \\ \leftarrow \text{row n} + N_m \end{matrix}$$

Defining:

$$B_{mn} = \sum_{a,r} D_{ar} \phi_{am} \phi_{rn} \quad ,$$

and:

$$\begin{cases} (n \neq m) & \epsilon'_{nm} = \dfrac{\omega_n B_{mn}}{\omega_n^2 - \omega_m^2} \\ (n = m) & \epsilon'_{nn} = \dfrac{-B_{nn}}{4\omega_n} \end{cases} \tag{23}$$

it is found that:

$$dR^o_{mn} = i\,\epsilon'_{nm}$$

$$dR'_{mn} = \begin{cases} i\omega_m\, dR^o_{mn} & \text{if} \quad m \neq n \\ -i\omega_n\, dR^o_{nn} & \text{if} \quad m = n \end{cases} \tag{24}$$

and thus the complex mode shapes are given by

$$\psi_n = \phi_n + i \sum_m \epsilon'_{nm} \phi_m \tag{25}$$

This shows that damping will in general result in complex modes. Finally, the second-order perturbation for the roots can be obtained by using in Eq. (4) the δR's given in Eq. (24), leading to the formulas:

$$\delta\omega_n = -\frac{B_{nn}^2}{8\omega_n} - \frac{1}{2} \sum_{m \neq n} \frac{B_{nm} B_{mn}}{2\left(\omega_n^2 - \omega_m^2\right)} \tag{26}$$

Other expressions may be obtained which show the dependency of ψ_n and $\delta\omega_n$ upon the feedback gains. If one defines (for the a-th actuator, r-th sensor, and m-th and n-th modes) the following quantities (the so-called Bizet coefficients):

$$K_{armn} \equiv \begin{cases} \dfrac{\omega_n}{\omega_n^2 - \omega_m^2}\, \phi_{am}\, \phi_{rn} & (m \neq n) \\ -\dfrac{1}{4\omega_n}\, \phi_{an}\, \phi_{rn} & (m = n) \end{cases}$$

the new (complex) modes ψ_{jn} (for the j-th node) are related to the original (real) modes ϕ_{jn} by

$$\psi_{jn} = \phi_{jn} + i \sum_{a,r} D_{ar} \left\{ \sum_m K_{armn}\, \phi_{jm} \right\} \qquad (i^2 = -1) \tag{25a}$$

and the corresponding perturbed modal frequencies are changed by:

$$\delta\omega_n = - \sum_{a,r,a',r'} D_{ar} D_{a'r'} \left\{ \frac{1}{8} K_{arnn} K_{a'r'nn} + \frac{1}{2} \sum_{m \neq n} K_{armn} K_{a'r'mn} \right\} \tag{26a}$$

Structural Transfer Functions

The modal equation of a structure containing damping devices may be written using Laplace transforms as:

$$\left[s^2 I + s\Phi^T D \Phi + \left[\omega_n^2 \right] \right] q(s) = \Phi^T F(s)$$

and Eq. (9) is written as

$$u(s) = \Phi q(s)$$

When the ζ's are small, so that the conditions of the low authority controllers apply, the following approximating expressions can be found for the transfer functions relating the effect of a force component F_a to the deflection u_r:

$$u_r(s)/F_a(s) = \sum_n \phi_{rn} [q_n(s)/F_a(s)] \tag{27}$$

where

$$q_n(s)/F_a(s) \cong \frac{\phi_{an} - s \sum_{m \neq n} \frac{B_{nm} \phi_{am}}{\left(s^2 + B_{mm} s + \omega_m^2\right)}}{\left(s^2 + B_{nn} s + \omega_n^2\right)} \tag{28}$$

These expressions are useful for evaluating the vibration of the structure induced by onboard excitation sources. When the excitation frequency is close to one of the mode frequencies, then $s^2 \cong -\omega_n^2$, and, since $B_{nn} = 2\zeta_n \omega_n$:

$$\left|u_r/F_a\right|_{\omega_n} \cong \frac{\phi_{rn} \phi_{an}}{2\zeta_n \omega_n^2} \tag{29}$$

By comparison, the static deflection (s = 0) is given by

$$\left|u_r/F_a\right|_o = \sum_n \frac{\phi_{rn} \phi_{an}}{\omega_n^2} \tag{30}$$

Generalized Modes and Force Distributions

So far the theory has been established for sensors measuring displacement (or velocities) and actuators applying local forces. The results may be extended to cases where sensors measure quantities such as local rotations, bending moments, etc., and where actuators produce a distribution of loads (such as doublets provided by torquers, moment actuators, etc.).

The sensor output y_r may be defined by a linear transformation of the type

$$y_r = \Sigma_j H_{rj} u_j \tag{31}$$

(For instance, in a one-dimensional structure,* the local rotation may be expressed as:

$$\theta_r = \frac{u_{r+1} - u_{r-1}}{\Delta x}$$

where Δx is the distance between stations $r+1$ and $r-1$.) Since $u = \Phi q$, the vector of sensor outputs may be written as:

$$y = \Phi^R q$$

where

$$\Phi^R \equiv H\Phi$$

is a matrix of generalized mode shapes.

---

*In a three-dimensional structure, "local rotation" mode shapes are obtained by "stacking" the three-dimensional curls $\vec{\nabla} \times \vec{\phi}_n$ of the deformation mode shapes. See Appendix B.

In the same way, an actuator controlled by a single input $f_a(t)$ may produce a distribution of loads:

$$f_{aj} = P_{aj} f_a(t) \tag{32}$$

where $j = 1, \ldots N_m$ is a station index. (For example, a torquer may be defined by $P_{aj} = 0$ except for $P_{aa-1} = -\Delta x$, $P_{aa+1} = \Delta x$, where Δx is the distance between station a-1 and a+1. In this case, $f_a(t)$ is the torque $T_a(t)$ produced by the torquer.)

The generalized rate feedback control law corresponding to Eq. (12) is now written:

$$f_a(t) = -\Sigma D_{ar} \dot{y}_r \tag{33}$$

and thus from (31) and (32)

$$f_{aj} = -P_{aj} \Sigma_{r,k} D_{ar} H_{rk} \dot{u}_k$$

Defining the generalized mode shape matrices Φ^A and Φ^R by:

$$\begin{cases} \Phi^A = P\Phi \\ \Phi^R = H\Phi \end{cases}$$

and the matrix B by:

$$B = \Phi^{A^T} D \Phi^R$$

all the formulas derived previously remain formally valid by replacing:

$$\begin{cases} \phi_{an} & \text{by} \quad \phi^{A}_{an} = \Sigma_j \, P_{aj} \, \phi_{jn} \\ \phi_{rn} & \text{by} \quad \phi^{R}_{rn} = \Sigma_j \, H_{rj} \, \phi_{jn} \\ B_{nm} & \text{by} \quad \Sigma_{a,r} \, D_{ar} \, \phi^{A}_{an} \, \phi^{R}_{rm} \end{cases} \tag{34}$$

In particular, the fundamental damping formula (16) becomes:

$$2\zeta_n \omega_n \cong \Sigma_{a,r} \, D_{ar} \, \phi^{A}_{an} \, \phi^{R}_{rn} \tag{35}$$

GYRODAMPERS

The preceding chapter addressed the general theory of low authority structural control dealing with the damped vibrations of flexible structures controlled by distributed systems of sensors and actuators with limited "damping authority."

The purpose of this chapter is to examine in detail the implementation of a specific type of inertial rotational damper, the so-called gyrodampers, with colocated angular rate sensors. This is an important class of devices, whose application to the control of large space structures appears very promising. Gyrodampers may be considered as momentum exchange devices between "local structural angular momentum" and gyro momentum. This exchange process involves rate-of-change of momentum, i.e., torque, so that these devices may also be regarded as torquers acting along the instantaneous axis of rotation of the deformable part of the structure to which they are attached. The torque applied by the gyros is electronically controlled so as to mimic the effect of a dashpot, i.e., opposing the rate-of-change of local angular rotation. Thus the structural vibration energy is dissipated in the form of heat radiated by the gyro's gimbal torque motors.

As will be shown in this chapter, the performance of these broad bandwidth devices provides substantial corroboration of the feasibility of achieving 10% to 20% structural damping with only a general approximate knowledge of the structure's modal characteristics.

Basic Principles

Consider a small rigid portion of an oscillating beam B , with an orthonormal frame $\{\vec{e}_1, \vec{e}_2, \vec{e}_3\}$ attached to it as shown in Figure 1. For simplicity of illustrating the basic principles involved, we assume that B can only undergo planar oscillatory

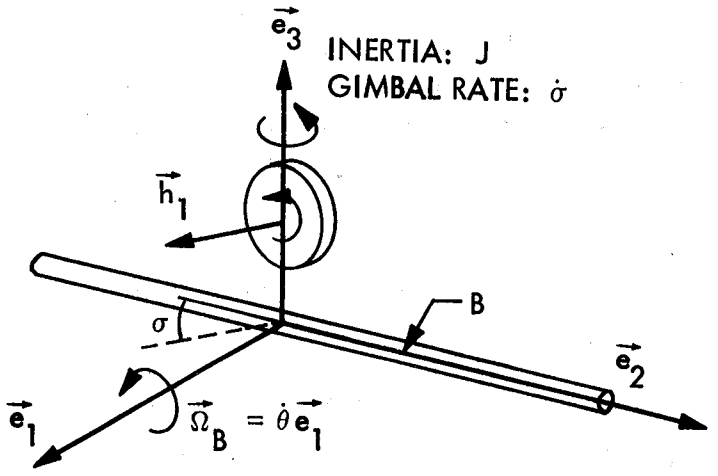

Figure 1. Section of beam with one gyro

rotations about $\vec{e}_1$, and that $\vec{e}_1$ maintains an inertially fixed orientation. Then the inertial angular velocity $\vec{\Omega}_B$ of B is

$$\vec{\Omega}_B = \dot{\theta}\vec{e}_1 \tag{36}$$

where θ is the angle of rotation of B about $\vec{e}_1$. A gyro, with constant speed rotor having angular momentum $\vec{h}$, is gimbaled on $\vec{e}_3$, the gimbal angle σ being zero when $\vec{h}$ is parallel to $-\vec{e}_2$. The total angular momentum $\vec{H}$ of the gyro, expressed in the moving frame $\{\vec{e}_1, \vec{e}_2, \vec{e}_3\}$ is then given by

$$\vec{H} = h(\sin\sigma\,\vec{e}_1 - \cos\sigma\,\vec{e}_2) + J\dot{\sigma}\vec{e}_3 \tag{37}$$

where $h \equiv |\vec{h}| = \text{const.}$, and J is the gyro's inertia about the gimbal axis $\vec{e}_3$.

Let $\vec{T}_g$ be the torque applied externally to the gyro. The equation of motion of the gyro is then:

$$\frac{d\vec{H}}{dt} = \vec{T}_g \quad , \tag{38}$$

where $d(\,)/dt$ denotes time differentiation w.r.t. inertial space. If $(\dot{})$ denotes time differentiation in the moving frame $\{\vec{e}_1, \vec{e}_2, \vec{e}_3\}$, and if we assume small motion linearized dynamics, then from (36), (37), and (38) we obtain:

$$\left.\begin{aligned} \frac{d}{dt}\left[h(\sigma\vec{e}_1 - \vec{e}_2) + J\dot{\sigma}\vec{e}_3\right] &= h(\dot{\sigma}\vec{e}_1 + \sigma\vec{\Omega}_B \times \vec{e}_1 - \vec{\Omega}_B \times \vec{e}_2) \\ &\quad + J\ddot{\sigma}\vec{e}_3 + J\dot{\sigma}\vec{\Omega}_B \times \vec{e}_3 \\ &\cong h(\dot{\sigma}\vec{e}_1 - \dot{\theta}\vec{e}_3) + J\ddot{\sigma}\vec{e}_3 = \vec{T}_g \end{aligned}\right\} \tag{39}$$

Assuming now that $\vec{T}_g \equiv T_g \vec{e}_3$ is a gimbal torque, projection of the last vector equation (39) along $\vec{e}_3$ results in

$$J\ddot{\sigma} = h\dot{\theta} + T_g \tag{40}$$

If, furthermore, $T_g \equiv -k\sigma - d\dot{\sigma}$, where $k > 0$, $d > 0$ are spring and dashpot constants, Eq. (40) represents a passive dissipative system driven by the input $\dot{\theta}(t)$. This passive gyro system will therefore absorb rotational energy by opposing the $\dot{\theta}$ motion. However, the transmission of this energy is determined by the magnitude of h/J, which, in most practical cases of oscillating beams or structures, is too small for effective damping.

Active Augmentation of Passive Gyrodampers

The inertial absorption of the $\dot{\theta}$-rotational energy by the passive gyrodamper is limited in practice by the magnitude of h/J. To increase this energy dissipation, an angular rate sensor is added to the system to estimate the $\dot{\theta}$ velocity which is fed-back to the gyro's gimbal motor with the proper gain so that the colocated sensor/actuator pair will mimic a purely passive device. As discussed in the Low Authority Structural Control Theory,* this passive nature alone guarantees structural stability, i.e., this (idealized) device cannot excite the structure, but the structure can excite it. Such an actively augmented passive damper can be caricatured as a passive device with a "hearing aid" to magnify the $\dot{\theta}$ signal, and in this sense, is quite distinct from a purely active device which does not necessarily require either a colocated sensor or a rate feedback.

The implementation of this concept will be illustrated for a system of two identical, coaxially gimbaled gyros (so-called V-gyros) as shown in Fig. 2. Indeed, the assumption in the previous example of Fig. 1 that $\vec{e}_1$ has an inertially fixed direction was only used for simplicity to idealize a simple 2 d.o.f. model using one gyro. In its quiescent state (i.e., $\dot{\theta} = 0$, $\sigma = 0$), the one-gyro model has a stored angular

*See Eq. (16)

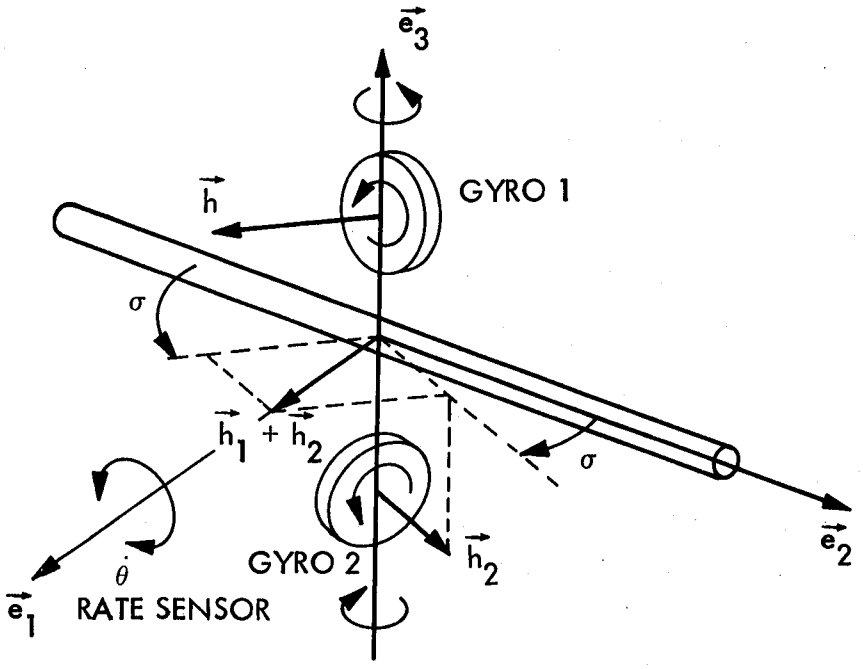

Figure 2. Section of beam with two coaxial V-gyros

momentum $\vec{h} \,/\!/\, -\vec{e}_2$, making the composite beam + gyro system a gyrostat, a generally undesirable characteristic. In addition, only infinitesimal gimbal motions will ensure that the body gyro torque $\dot{\vec{h}}$ is aligned with the $\dot{\theta}$-input axis $\vec{e}_1$ for damped momentum exchange between beam $\dot{\theta}$-oscillations and gyro gimbal motions.

When two identical gyros are used such that zero gimbal angles correspond to gyro momenta alignments $\vec{h}_1 \,/\!/\, -\vec{e}_2$ and $\vec{h}_2 \,/\!/\, \vec{e}_2$ (see Figure 2), then the counter-rotation of the rotors cancels the internally stored momentum. In addition, because of symmetry, the $\dot{\theta}$-induced gyro gimbal motions result in the classical "V-scissor" pairing of the momenta $\vec{h}_1$ and $\vec{h}_2$; i.e., the resultant total gyro momentum (w.r.t. the frame $\{\vec{e}_1, \vec{e}_2, \vec{e}_3\}$) always remains aligned with the $\pm\vec{e}_1$ beam axis. This allows utilization of increased gyro gimbal travel. Of course, this travel is limited in practice due to the nonlinear relation between gyro momentum and gimbal angle, i.e.,

$$(\vec{h}_1 + \vec{h}_2) \cdot \vec{e}_1 = 2h\sin\sigma \tag{41}$$

where $h \equiv |\vec{h}_1| = |\vec{h}_2|$.

For each gyro, Eq. (40) remains valid, but the gimbal torque T_g is no longer realized by passive springs and dashpots, but generated electronically by gimbal motors and will include a feedback term proportional to the sensor output $\dot{\theta}$. The gyrodynamics (see Eq. 40) of each gyrodamper are now described by:

$$J\ddot{\sigma} = h\dot{\theta} + \overbrace{(K\dot{\theta} - d\dot{\sigma} - k\sigma)}^{\text{feedback loop}} \equiv T_G \tag{42}$$

and the output ("vehicle") torque applied to the beam by the gyros (see Eq. 41) is given by:

$$\begin{aligned} T_V &\equiv -(\dot{\vec{h}}_1 + \dot{\vec{h}}_2) \cdot \vec{e}_1 = -2h\cos\sigma\dot{\sigma} \\ &\cong -2h\dot{\sigma} \end{aligned} \tag{43}$$

The gain k in (42) represents a weak spring ensuring a zero dc value of the gimbal angles σ. The classical gyroscopic torque $\vec{\Omega}_B \times \vec{h}$, where $|\vec{\Omega}_B| = \dot{\theta}$, occurs on the gyro gimbal axes and appears as $h\dot{\theta}$ in Eq. (42). (This torque would normally drive the gyro gimbals in a purely passive system.)

For preliminary design purposes, the gains in the feedback term $K\dot{\theta} - d\dot{\sigma}$ in Eq. (42) are made large enough for the dynamics of the gyro itself to become negligible (i.e., the $J\ddot{\sigma}$ inertial effect), ensuring $\dot{\sigma} \sim [(K + h)/d]\,\dot{\theta}$, so that Eq. (43) becomes:

$$\left.\begin{aligned} T_V &= -D\dot{\theta} \\ D &\equiv 2h(K + h)/d \end{aligned}\right\} \qquad (44)$$

where D can be interpreted as the damping constant of an ideal θ-damping torquer attached to inertial space. This interpretation reflects the fundamental property of gyrodampers used as inertial energy sinks, or equivalently, as inertial dampers, in contradistinction to intrastructural dampers (e.g., shock absorbers) connecting two distant points of the beam or structure in general.

The above considerations become more quantitative by introducing the gyrodamper transfer function (see Figure 3) corresponding to Eq. (42):

$$\left.\begin{aligned} \sigma/\theta &= \frac{iK'\omega}{\omega_G^2 - \omega^2 + i\omega_1\omega} \\ \text{where} \qquad K' &\equiv (K + h)/J \\ \omega_1 &\equiv d/J \\ \omega_G^2 &\equiv k/J \\ i^2 &= -1 \end{aligned}\right\} \qquad (45)$$

The gyrodamper bandwidth is the interval $[\omega_o, \omega_1]$, where

$$\omega_o \equiv \omega_G^2/\omega_1 \qquad (46)$$

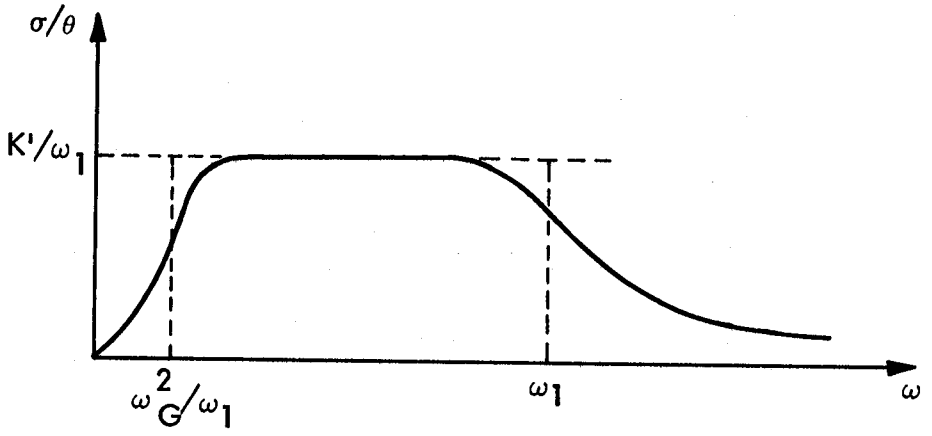

Figure 3. Gyrodamper transfer function

Since k is a weak spring, ω_o is small. On the other hand, ω_1 is chosen large enough to include the highest structural frequency which must be damped. Within this bandwidth,

$$|\omega_G^2 - \omega^2| \ll \omega_1 \omega$$

so that the transfer function (45) reduces to

$$\sigma/\theta \cong K'/\omega_1$$

Thus Eq. (44) can now be expressed as:

$$\left.\begin{aligned} T_V &= -2h\dot{\sigma} = -D\dot{\theta} \\ D &\equiv 2hK'/\omega_1 \end{aligned}\right\} \quad \text{(44a)}$$

where

Beam Damping Simulations

Physical and Mathematical Model. To illustrate specifically the (theoretically predicted) performance of an inertial rotational damper, the V-CMG damping system shown in Figure 4 was rigorously modeled on Lockheed's multibody hybrid coordinate software (ref. 4). The model included both the noise produced by the $\dot{\theta}$ rate-sensing unit (e.g., rate sensing gyros, not shown) and the effects of gyro vibration due to rotor mass imbalance.

The physical model used (Figure 4) is a 10-m tubular aluminum beam, 10-cm diameter, 2-cm thick, whose mass is 136 kg. A horizontal V-CMG damper unit is clamped at its center, with the gyros mounted back-to-back in the nominal (zero momentum) configuration. For each gyro, the rotor inertia about the shaft is $J_s \sim 0.021$ kg-m^2, while the transverse inertia J (including gimbal inertia) is slightly over half that amount. The mass of each rotor is 3 kg, its diameter is ~ 15 cm, and its spin-rate is 400 rad/s (~ 4000 rpm) so that the angular momentum of each gyro is h = 8.4 N-m-s (~ 6.2 ft-lb-s). Additional physical parameters are shown in Figure 4.

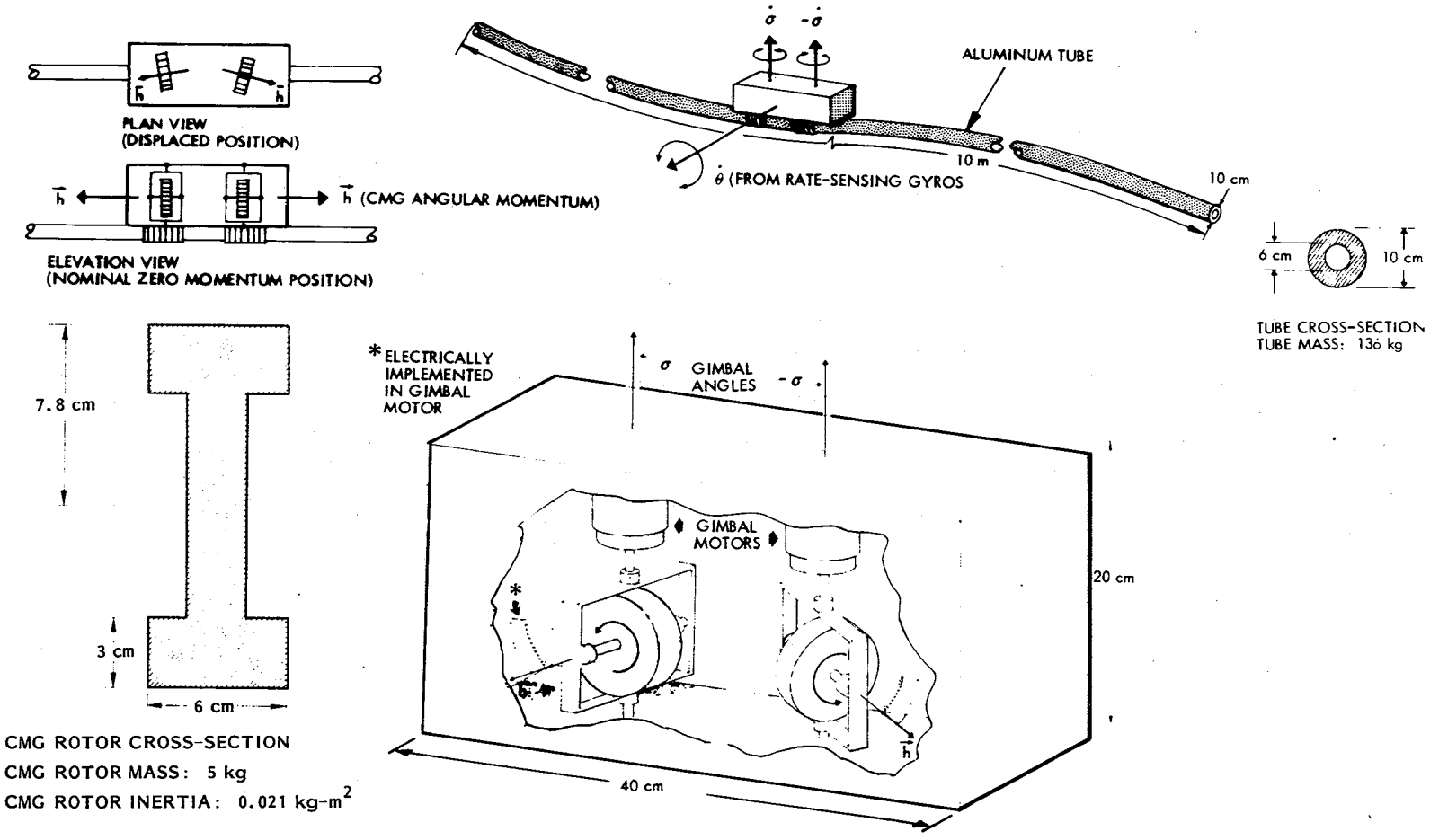

Figure 4. V-CMG inertial damper producing single-axis damping torque

The mathematical multibody hybrid coordinate model used consists of five bodies: The "damping unit box", two identical single-gimbal gyros, and two 5-m cantilevered tubular beams abutted end-to-end under the damping unit. Because the motion equations of this system constitute a precise evaluation model which must include the actuator dynamics, the first six (planar) cantilever beam modes were included for each beam, in addition to one rigid body mode (damper box rotation about the θ-axis), and 2 degrees of freedom for each gyro (gimbal angle σ and rotor phase angle, an ignorable coordinate). This 17 degree-of-freedom system was modeled open-loop in the nonlinear N-BODY program, with the gyro gimbal control torque and θ-input torque treated as external inputs. Using the built-in numerical linearization procedure, the constant coefficient matrices of the corresponding linearized (first-order form) model were then input to state-space linear systems software (LISSA 6), where the control loop was closed. The control equation is linear and relates the gimbal torque to the angular rate $\dot{\theta}$ of the device and also to the gimbal angle σ and rate $\dot{\sigma}$. This last variable is necessary to make the gyro system behave like a passive rotational damper.

Briefly, in the subset of hybrid linear equations corresponding to the variables θ and σ, the rate-sensor feedback loop was closed as follows:

$$\left.\begin{aligned} &\underline{\text{Total System:}} \quad I\ddot{\theta} = -2h\dot{\sigma} + T(q) \\ &\underline{\text{Each Gyro:}} \quad J\ddot{\sigma} = h\dot{\theta} + \underbrace{(K\dot{\theta} - d\dot{\sigma} - k\dot{\sigma})}_{\text{feedback loop}} \end{aligned}\right\} \tag{47}$$

where I is total (beam + gyros) θ-inertia, and T(q) is a linear combination of "system modal torques" produced by the antisymmetric vibrations of the beam. The q's are the modal amplitudes associated with the beam mode shapes included in the simulation. (See Appendix A for a complete description of the nonlinear actuator dynamics for a free-free beam equipped with an arbitrary number of V-gyrodamper units.)

Design and Tuning Procedure

The first step in the design procedure is to determine the value of the damping gain D which will give desired performance for an ideal torquer. This can be obtained either from the fundamental prediction formula (16) or from parametric simulation studies of the actual system. Using the latter, a damping gain $D = 1{\cdot}2\ 10^4$ N·m·s was found desirable. To implement this with the gyro-damper described earlier ($h = 8.4$ N·m, $J = 0.01$ kg m^2) with a desired bandwidth $\omega_1 = 1400$ rad/sec (about twice the frequency of the highest mode to be controlled), Eqs. (44) and (45) are used to determine the two control gains:

$$d = J\omega_1 = 14 \text{ N·m·s}$$
$$K = \frac{Dd}{2h} - h \cong 10^4 \text{ N·m·s} \tag{48}$$

Without this feedback loop, the equivalent damping gain of the passive system would have been $D = 10.1$ N·m·s.

Numerical Simulation. The automated modeling procedure is a generalization of the "two-stage eigenanalysis" method used by Draper Laboratory (ref. 5) in that the original model includes not only structural modes, but also the dynamics of other components of the system (e.g., interconnected bodies, gyros, etc.). Of the 34 (complex) eigenmodes corresponding to the original 17 degrees of freedom physical system, 12 system modes are essentially the first 12 classical free/free-beam modes. Because the damper unit is located at the exact center of the 10-m beam, the six symmetric modes are undamped. Of the remaining six antisymmetric modes, only the first three are physically meaningful because of bandwidth limitations (~ 100 Hz) inherent to rate-sensing gyros needed for the $K\dot{\theta}$ feedback term in Eq. (47). The corresponding system modal frequencies, damping coefficients and decay time are listed in Table 1.

TABLE 1. SYSTEM MODAL DAMPING

Frequency (Hz)	Damping (%)	Decay Time (s)
19.9	15.09	0.053
57.8	5.35	0.051
113.9	2.93	0.048

This system was simulated for 1 s, the initial conditions being a 1-mm deflection of the beam tips in opposite directions. This static deflection was decomposed in the original cantilever modal basis to obtain the initial conditions $q_n(0)$ for the beam modal amplitudes in the closed-loop hybrid linear system. The ensuing damped oscillations of the tip-deflection and its modal components $q_n(t)$ are shown in Figure 5 for the first 0.5 s of simulation. Without sensor or actuator noise, tip deflections diminish to a few millimicrons at 1 s, an interesting but not physically meaningful result. In practice, sensor and actuator noise drive the gyro damper as an active excitation source. However, the resulting vibrations turn out to be below the level required by precision space structures. (For optical or rf systems, this level varies between 1/10 to 1/50 of the wavelength.)

With rate-sensor noise (obtained from bandpass filtered white noise) having mean amplitude ~ 0.5 μrad/s (an order of magnitude higher than for the best rate-sensing gyros), the residual tip-deflections between 0.9 s and 1 s average a few hundredths of a micron. This noise, and its effect on tip-deflection, gyro gimbal torque, and spurious θ-damping torque are shown in Figure 6. For actuator noise due to gyro rotor vibration, one compliant bearing was assumed for each gyro to allow the coning motions of the rotor shaft due to a typical 1-μin. ($\sim 2.5\ 10^{-8}$m) mass-center offset of the rotor. The resulting level of spurious damping torque ($\sim 16\ 10^{-4}$ N-m) is about half the peak amplitude of the spurious component due to sensor noise (Figure 6). Finally, the time-histories $\theta(t)$ and $\sigma(t)$ are shown in Figure 7. These results are scalable (using larger gyros) to different vibration levels.

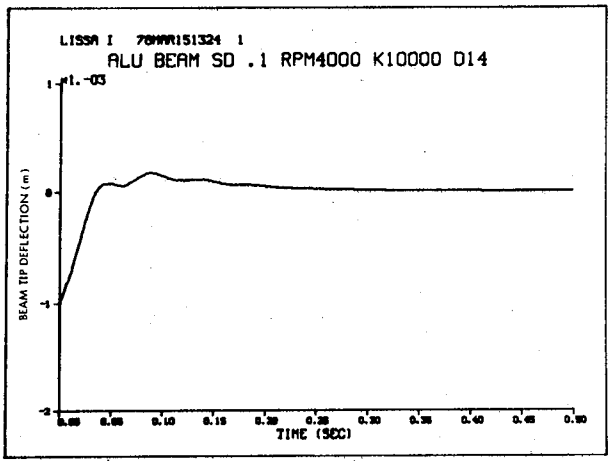

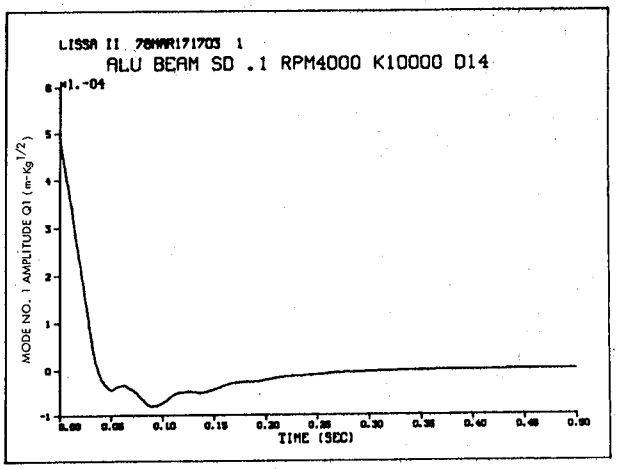

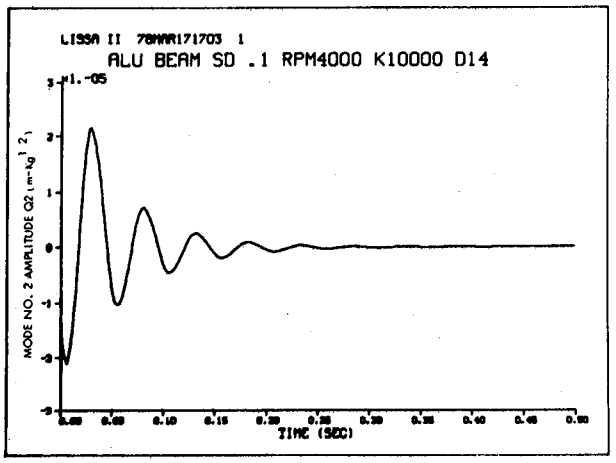

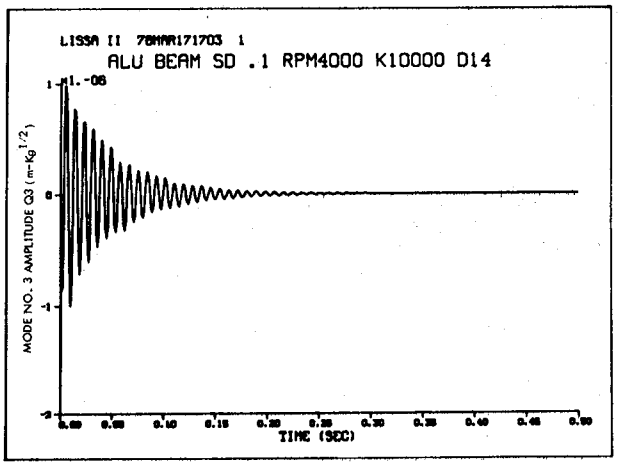

Figure 5. Gyro damper performance

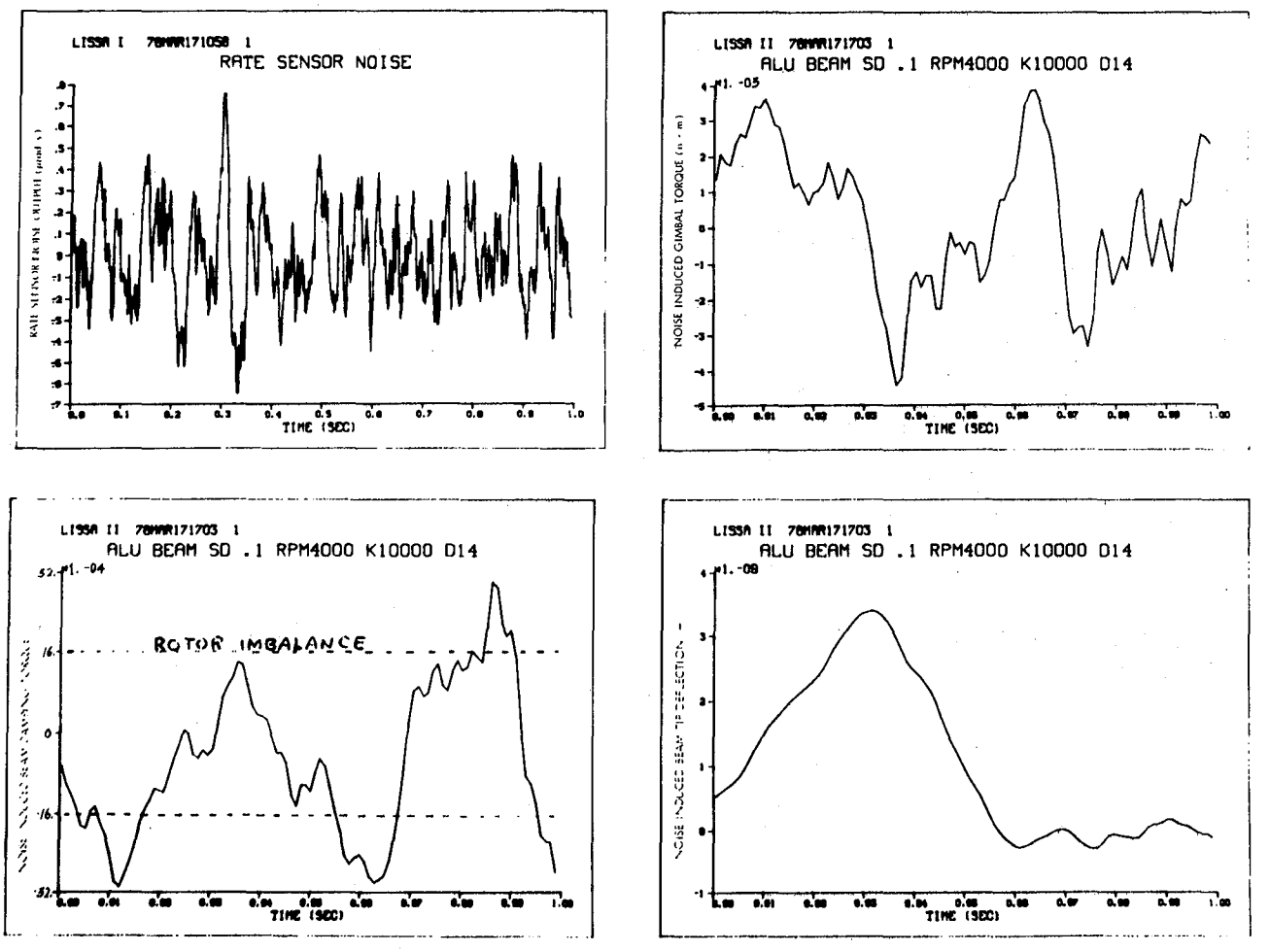

Figure 6. Effect of rate sensor noise and rotor imbalance on gyrodamper performance

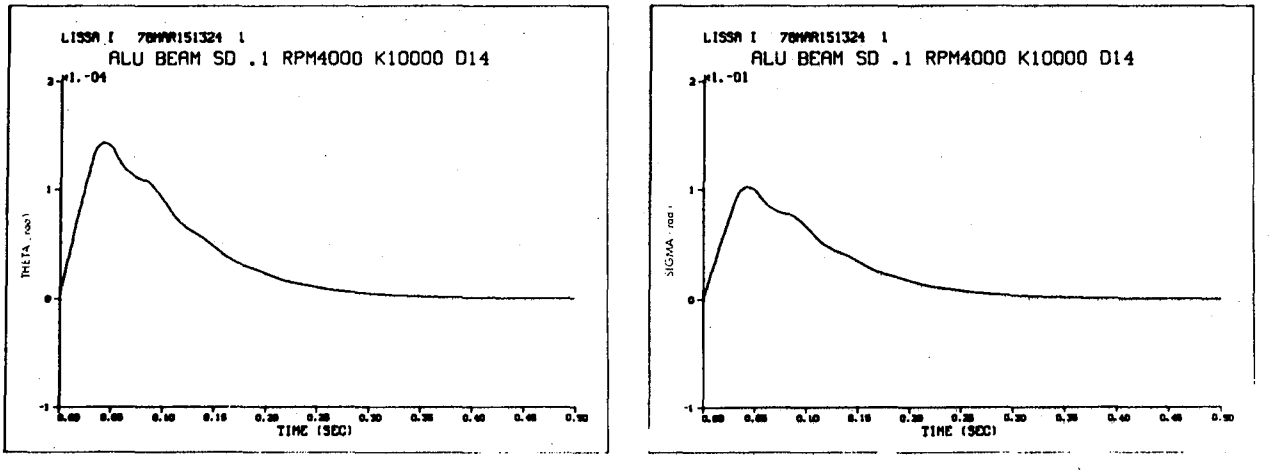

Figure 7. Local beam rotation and gyro gimbal angle

Gyrodamping of a 100-m GrEp Beam

The simulation studies described in the previous subsection established feasibility of the V-gyrodamping of a relatively massive, thick and stiff aluminum 10-m tube, including rate sensor noise and gyro-rotor imbalance effects. The damping unit was placed at the exact center of the beam, thus leaving (by definition) the symmetric modes undamped. In addition, Lockheed's general-purpose multibody hybrid coordinate software (in the sense of Likins) was used, requiring cantilever mode shapes for each half of the beam "clamped" under the centrally located V-gyrodamper unit.

As can be inferred from the previous example, the numerical methodology employed is relatively complex. This follows from the use of generalized multipurpose software constrained to use cantilever modes for flexible structures attached (or gimbaled) as terminal "appendages" to arbitrary topological trees of interconnected rigid bodies. With this software, a flexible beam with a (relatively) small-mass V-gyrodamper attached at one end can still be modeled, but an excessive number of higher order cantilever modes are required to converge to a physically useful set of free-free modes, as was done in the first example of the massive tubular aluminum beam. This numerical phenomenology can be loosely identified as the pathology of the "tail wagging the dog." Because of this phenomenology (in addition to numerous other reasons derived from the rapidly evolving design changes associated with current and future large space structures), development of a new generation of "multibody" software was initiated under the Lockheed Independent Research program these last few years. The basic idea involved is the "turning inside-out" of the original hybrid coordinate topological tree model originally developed in 1965 by Hooker and Margulies, and subsequently extensively studied and documented by Likins and many others (Ref. 6).

Briefly stated, the "inside-out" model consists, in the first phase, of a single free-free flexible structure, having large-angle rigid-body modes, and containing an arbitrary number of arbitrarily gimbaled rigid bodies to model reaction wheels, gyros,

gimbaled variable-speed wheels, etc. (In the second phase, additional gimbaled flexible appendages will be attached to the main flexible body.) Because of the mathematical complexity of these models, only equations of motion for a simple "submodel" are given in Appendix A. This submodel is limited to the planar vibrations of a free-free flexible beam equipped with an arbitrary number of arbitrarily located V-gyrodamper units.

To illustrate this unique simulation capability, a second example of a large 100-m graphite epoxy beam equipped with one and two V-gyrodamper units was considered, including comparisons between damper locations, low authority structural control, and "ideal torquer" simulations, and the effects of nonlinear gyro actuator dynamics. The physical parameters of the beam were chosen as follows:

Length	$L = 100$ m
Outside Radius	$r = 10.55$ cm
Wall Thickness	$e = 2.275$ mm
Young's Modulus	$E = 3.45\ 10^{11}$ N/m^2
Density	$\rho = 1607$ kg/m^3
Mass	$M = 239.7$ kg
Sectional Inertia	$I = 8.125\ 10^{-6}$ m^4

$$K_S = (EI)^{-1/2} = 5.973\ 10^{-4} \quad \text{kg}^{-1/2}\text{-m}^{-3/2}\text{-s}$$

The V-gyrodampers used on the above beam were chosen to have the following (conservative) characteristics (for each V-gyrodamper unit):

Total damper unit mass	$m = 8$ kg
Gimbal Inertia	$J = 0.021$ kg m^2
Rotor Spin Rate	$\Omega = 400$ rad/s
Rotor Angular Momentum	$h = 8.4$ N-m-s
Maximum Gimbal Torque	$T_G = 3.2$ N-m
Peak Power	$P_p = 8$ W
Maximum Gimbal Angle	$\sigma_{max} = 1$ rad

Maximum Gimbal Rate	$\dot{\sigma}_{max} = 2.5$ rad/s
Maximum Gimbal Acceleration	$\ddot{\sigma}_{max} = 40$ rad/s^2
Feedback Gains #	$K = 10^4$ N-m-s/rad
	$d = 6.27$ N-m-s/rad

In the first simulation example of the aluminum tubular beam, time histories were displayed for all the physically relevant system variables, i.e.,

- Beam tip deflection
- First three modal amplitudes
- Rate sensor noise output
- Noise-induced gyro gimbal torque
- Noise-induced beam damping torque (including effects of gyro rotor imbalance)
- Noise-induced beam tip deflection
- Rigid body mode beam rotation
- Gyro gimbal angle travel

Because of the multivariate aspect of the problem, results for the GrEp beam will be limited* to time-histories of the modal amplitudes of the first two free-free beam modes (first symmetric q_1, first skew-symmetric q_2). From these modal amplitudes one can reconstruct either the beam deflections $u = \Sigma_n \phi_n q_n$ or the local rotations $\theta = \Sigma_n \phi'_n q_n$. (See Appendix B.) For all the simulations shown, the initial conditions for the q's were obtained by decomposing a 1-cm beam tip deflection into the free-free beam modal basis.

Figure 8 (b), (c), (d) shows the comparison between nonlinear actuator dynamics, low-authority structural control algorithms, and the ideal torquer model interpreted as the application of a damping torque directly against inertial space. (For practical purposes, this model corresponds essentially to linear actuator dynamics with infinite bandwidth.) There is a perfect match between this model and the low-authority control algorithm [Figure 8 (c) and (d)], while the "modulation" occurring around 1.75 s

---

#K and d were obtained as in (48), for the new value of J.

*The remaining system variables have essentially the same qualitative behavior as in the first aluminum beam example.

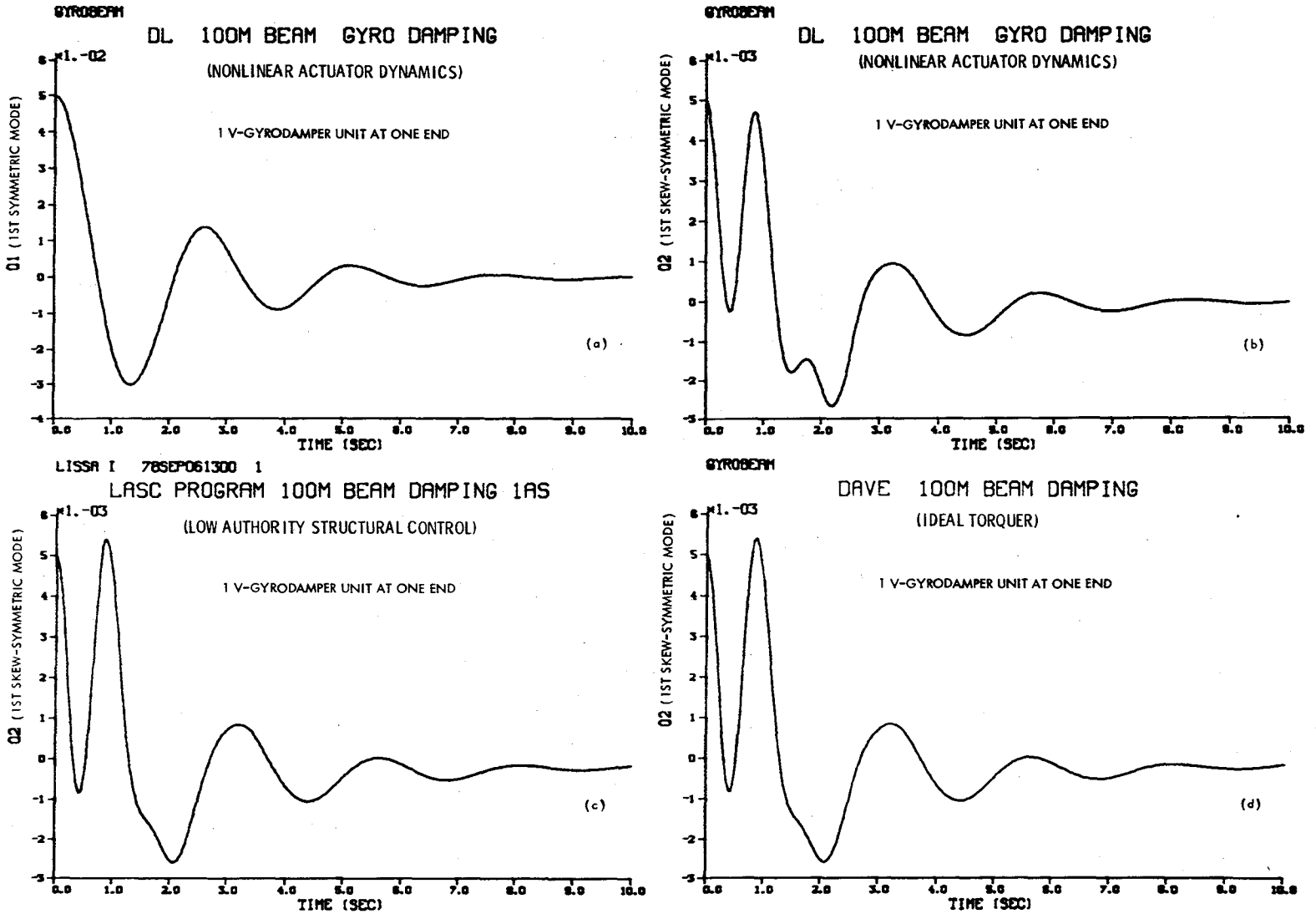

Figure 8. Gyrodamping of a 100-m GrEp beam — comparison between nonlinear actuator dynamics, low authority structural control, and ideal torquer dynamics.

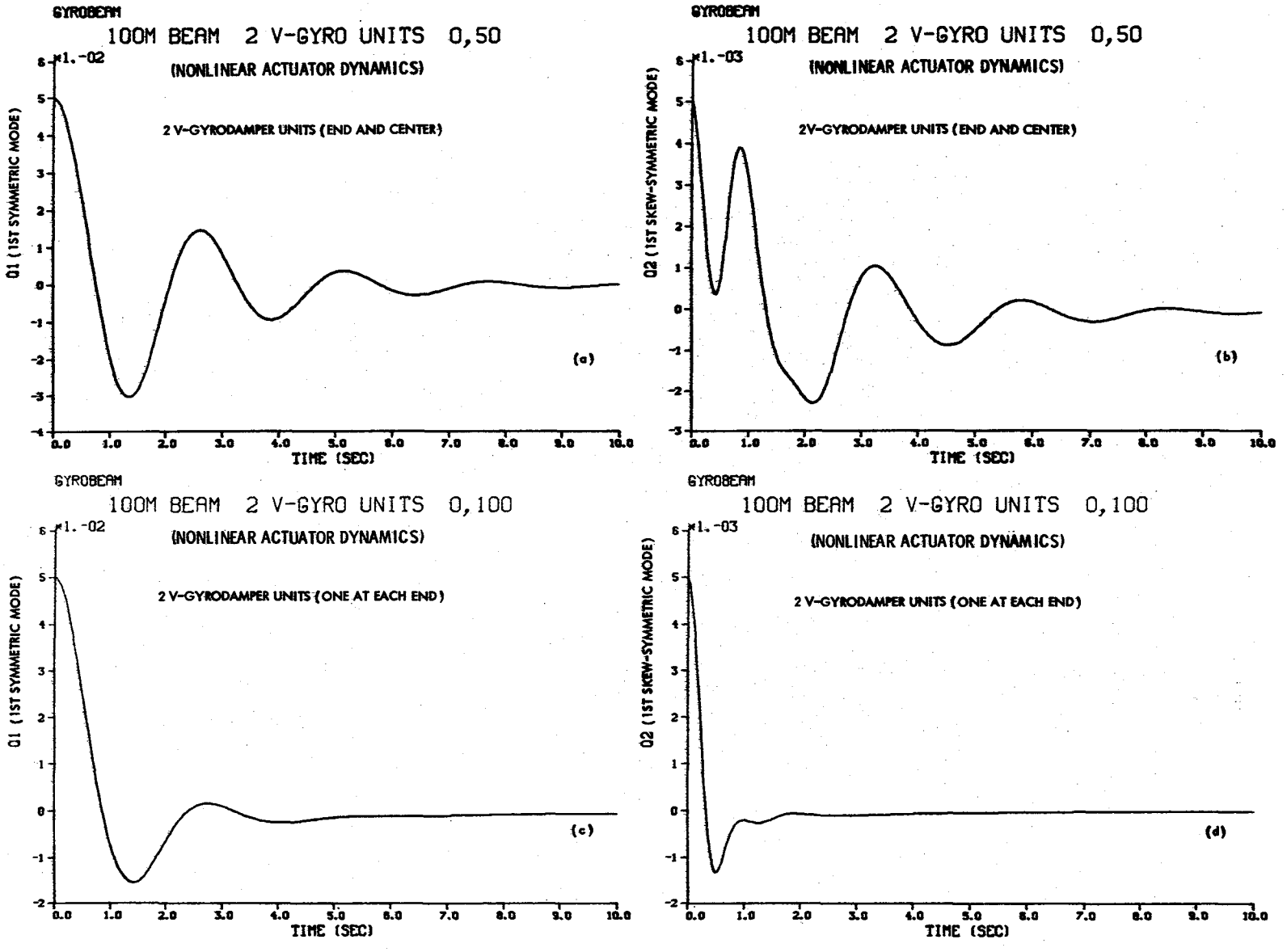

Figure 9. Gyrodamping of a 100-m GrEp beam — comparison between location of two damping units for first two modal amplitudes.

for the nonlinear actuator dynamics corresponds to a momentary gyro momentum saturation. Figure 8 (a) shows the effect of nonlinear actuator dynamics on the first mode, which exhibits approximately 19% damping, in accordance with the theoretically predicted values as shown in Table 2. The difference between predicted and actual values is due to the relatively high level of required damping.

TABLE 2. SYSTEM MODAL DAMPING

System Mode No.	Freq. (Hz)	Predicted Damping (%)[a]	Actual Damping	Actual Decay Time (s)
1	0.405	19.66	19.2	2.04
2	1.14	19.66	13.6	1.03
3	2.05	19.66	8.7	0.89
4	3.04	19.66	6.0	1.14

(a) Obtained from Eq. (65).

Figure 9 shows the comparison between V-gyrodamper locations when two units are used, via their effect on the first two modal amplitudes. As can be intuitively expected, the centrally located unit has essentially no effect on the first symmetric mode [compare Figure 8 (a) with Figure 9 (a)], and some effect on the first skew-symmetric mode [compare Figure 8 (b) with Figure 9 (b)]. The smallness of this effect reflects the considerably smaller strain energy stored in this mode as compared to the first symmetric mode for the chosen initial condition of 1-cm beam tip deflection. Also, because the introduction of damping into the system couples the modal amplitudes, the transients in all the simulations shown are essentially dominated by the first symmetric mode. Finally, Figures 9 (c) and 9 (d) show the radical improvement when the two gyrodampers units are placed one at each end of the beam. This again is in agreement with physical intuition in that the maximum slope changes will occur at the ends of a free-free beam.

Gyrodampers for 3-D Structures

The V-gyrodampers discussed in the previous sections are an example of gyroscopic single-axis damping of planar beam vibrations for which these units were

designed. If transverse beam vibrations were also present, the gyros would keep their individual momenta antiparallel (total zero momentum), and therefore would not participate in transverse beam vibrations except through a weak gimbal inertia effect. For two- or three-dimensional vibrations, different gyrodamping configurations are required, and many combinations are possible. In particular, two single-axis V-gyrodampers, clamped on the same beam with their gimbal axes at right angles, would extend the damping procedure for planar vibrations to both planar and transverse beam vibrations in a simple, essentially decoupled way.

For two-dimensional beam vibrations, the damping torques which must be applied by the gyros will span a plane orthogonal to the beam. The two orthogonal V-gyrodamper units mentioned above are thus a particular implementation of a two-axis torque control system. There exist many other gyro configurations for two-axis control. For instance, two V-gyrodampers may be arranged with their gimbal axes parallel (i.e., orthogonal to the control plane) and such that the "scissoring" motion of each pair occurs along perpendicular axes in the control plane, as shown in Fig. 10a. An important quantitative characteristic of any gyro system is its momentum envelope (ref. 7), i.e., the set of all its achievable angular momenta. For the configuration in Fig. 10a, this momentum envelope is a square of side 4h, provided that $\pm 90°$ gimbal travel is allowed for all gyros. However, if the four gyros are not paired but made independent, a larger momentum envelope is obtained, i.e., a disk of radius 4h, as shown in Fig. 10b. The increase (by a factor π) of the momentum envelope area must be traded off against the increased complexity of the damper actuation control laws. Finally, it can be shown that three independent coaxial gyros (whose momentum envelope is a disk of radius 3h) is sufficient to achieve 2-axis control. However, the requirement of unlimited gimbal travel in conjunction with bandwidth limitations may lead to unfeasible implementations of such configurations whose main advantage is reduced damper mass (three gyros instead of four, grouped in two V-pairs). These are open questions at present, and would require further in-depth study.

When the most general case of a large space structure is considered, deformations of a local material neighborhood are such that the instantaneous rotation vector may take any direction in space. This is the case, for example, when planar shearing modes of a platform are considered. The instantaneous rotation vector is then normal

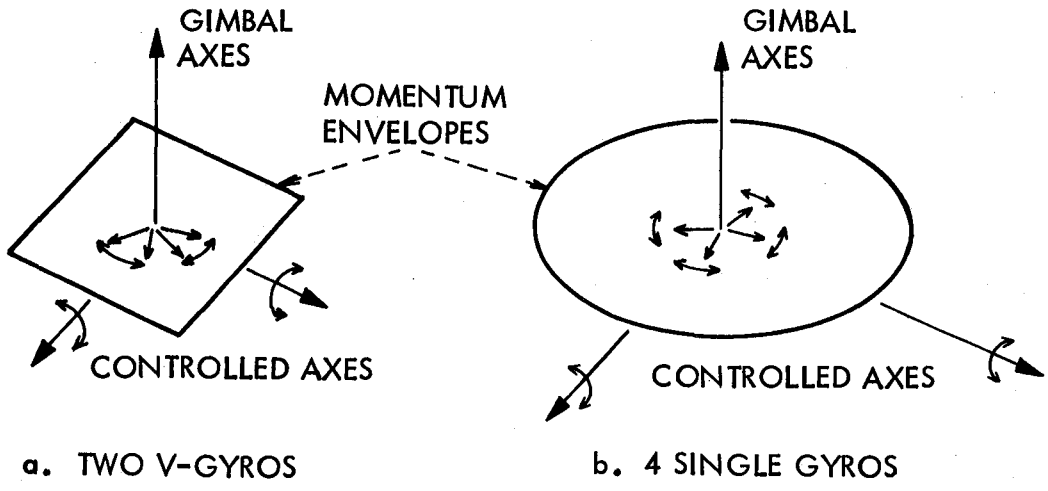

Figure 10. Momentum envelopes for 2 V-gyros and 4 single gyros

to the platform, while for bending or twisting modes it is essentially tangent to the platform. A gyrodamper configuration for this application must therefore be capable of achieving 3-axis (damping) torque control, and hence its momentum envelope must be a three-dimensional region. Here again, three pairs of orthogonally mounted V-gyrodampers may offer the simplest implementation of controller actuation, with a momentum envelope being a cube of side 4h. If these units can be mounted on the edges or corners of a large platform, within easy reach of the Shuttle for replacement, the failure-reliability problem is alleviated. If not, failure of any single gyro automatically disables the V-pair to which it belongs, resulting in loss of control of one axis.

A general approach to using six gyros for three-axis control is to abandon the concept of V-pairs, and mount them as independent gyros whose gimbal axes are equidistributed along the generators of a cone, as shown in Figure 11. The corresponding momentum envelopes are shown in Figure 12 for the case of zero, one, and two gyro failures.* With no failures, and for a 30° cone half-angle, the momentum envelope is an oblate spheroid of equatorial diameter 11.21 h and polar diameter of 6 h. In addition to the increased momentum capability of this configuration, these conical systems of gyros, none of which play a preferred role, can be made inherently tolerant to successive device failures, with minimum loss in system performance. However, special control laws are required to achieve this, and a tradeoff between complexity of implementation and structural bandwidth constraints must be analyzed. In the context of attitude control, on-going studies funded by the Lockheed Independent Reasearch Program have documented the formulation, development, and design of nonlinear optimal control laws for arbitrary systems of identical single-gimbal control moment gyros. There appears to be a direct applicability of this technology to NASA's interest in the control of large space structures, in particular when the attitude control and structural control problems must be synthesized. While these problems are outside the scope of the present study, it is quite conceivable that dual-purpose gyro systems can be designed to solve the attitude and structural control synthesis problem.

---

*These envelopes are boundaries of almost convex regions; inside the white holes, the surface folds inward slightly, resembling a shallow depression. Since the surface is represented by a curvilinear parameter net, and since this net becomes singular inside the white holes, inside details are not show. For further details on this point, see Ref. 7.

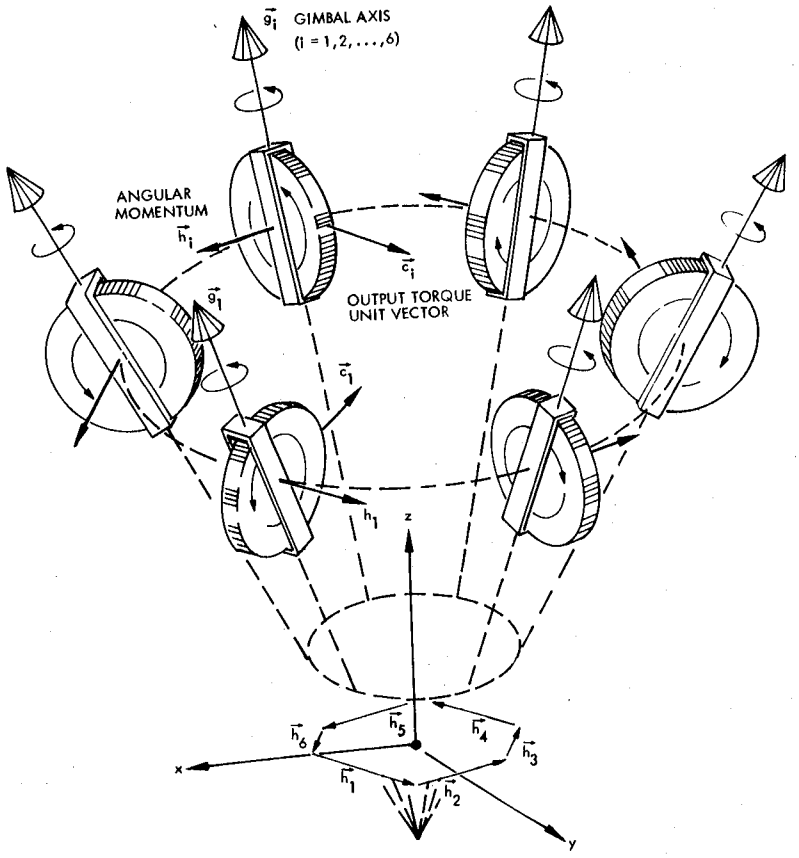

Figure 11. Six CMGs with gimbal axes equidistributed along the generators of a cone

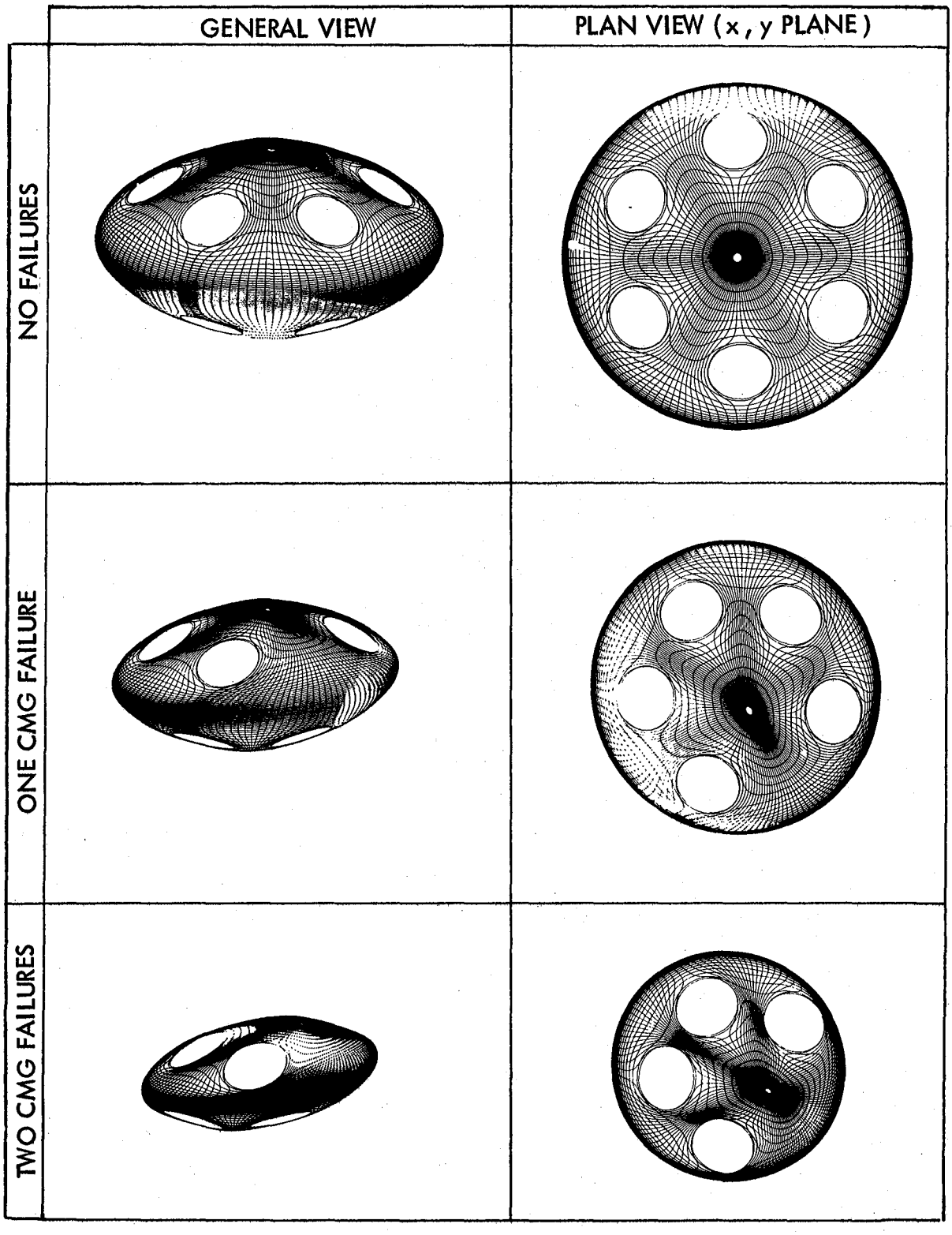

Figure 12. Two views of the angular momentum envelopes of the 6-CMG cluster (corresponding to conical array of 6 CMGs shown in Figure 11)

SCALING LAWS

The purpose of this chapter is to define the basic parameters that determine the performance of a structure controlled by gyrodampers, and obtain formulas enabling the designer to extrapolate the results obtained with a particular structure/gyros combination to a structure of different characteristics.

Scaling Parameters for Control Moment Gyros

Control moment gyro system performances are limited by four basic constraints:

(1) The gimbal angle σ : limited because of the nonlinear characteristic of the gyros. For instance, for V-gyros, the output torque is proportional to $2h\cos\sigma$; thus for σ near 90°, the system becomes very ineffective.

(2) The gimbal angular rate $\dot{\sigma}$: limited because the output torque ($\cong h\dot{\sigma}$) has to be transmitted from the wheel to the shaft and is thus only as good as whatever structural part connects the rim to the shaft.

(3) The gimbal angular acceleration $\ddot{\sigma}$: limited because the maximum torque available from the gimbal motor has to overcome the inertia about the gimbal axis of the gimbal/wheel/spin-motor combination.

(4) The dissipated power P_p : limited by the heat dissipation capabilities of the gimbal torque motor.

Given these four constraints, the optimum gyro will be the one with the greatest possible momentum h . On the other hand, the mass of the total damper device should be minimum. Therefore, the following problem must be addressed: assuming that for a given mass m , some sort of "optimal" design has been achieved, how is the performance of the system affected by choosing a different mass? The materials used being assumed the same, the problem is equivalent to choosing a different characteristic length, ℓ , of the system. Under these conditions of pure geometric

scaling, it will be shown that there exist some invariant quantities, called henceforth the gyro scaling parameters (GSP), which relate some fractional powers of the mass to the gyro characteristics and performance.

Very simple physical considerations need to be introduced, bearing in mind that, under this geometric scaling, the mass of any one part stays proportional to the total mass m. First, the inertia J_{3_s} of the wheel about its spin axis is proportional to $m\ell^2$, and since m varies with ℓ

$$J_s = C_1 m^{5/3} \tag{49}$$

(The symbols C_1, C_2, etc, ..., designate constants invariant under geometric scaling.) The same type of relation holds also for the total inertia J about the gimbal axis.

Next, calling Ω_s the spin rate, the centrifugal force on the rim is $\sim m\Omega_s^2\ell$. Since material strength is $\sim \ell^2$, it is necessary that $\Omega_s^2\ell^2 \leq C_2$.

Since $h = J_s \Omega_s$, this may be written as:

$$h^2\ell \leq C_2 J_s^2$$

and using (49) shows that the maximum achievable momentum is

$$h = C_3 m^{4/3} \tag{50}$$

Now the output torque, $h\dot{\sigma}$, being limited by the wheel/shaft/bearing strength, is such that

$$h\dot{\sigma} \leq C_4\ell^2$$

Combining this with (50), an expression for the maximum gimbal rate is

$$\dot{\sigma}_{MAX} = C_5 m^{-2/3} \tag{51}$$

Some consideration is now given to the electrodynamic actuator. In a classical type, it is assumed here that the force produced is proportional to V/R_t, where V is the applied voltage, R_t the resistance of one winding of length $2\pi d$. Since $R_t = \rho\, 2\pi d/s \sim 1/\ell$, where ρ is the resistivity of the conductor and s its cross-sectional area, the torque T_G produced on the gimbal is then

$$T_G = C_6 m^{2/3} \tag{52}$$

(If the current, instead of the voltage, was maintained constant, T_G would then be proportional to $m^{1/3}$.) Finally, the maximum power is determined by the heat dissipation which would be related to radiating surfaces, and thus

$$P_p = C_7 m^{2/3} \tag{53}$$

It is convenient to express Eqs. (49) to (53) in terms of the following gyro scaling parameters:

Gyro Scaling Parameters (GSP)

			SI Units
$K_{J_s} = J_s^{-1}$	$m^{5/3}$	(spin inertia)	$Kg^{2/3}\, m^{-2}$
$K_J = J^{-1}$	$m^{5/3}$	(gimbal inertia)	$Kg^{2/3}\, m^{-2}$
$K_H = h$	$m^{-4/3}$	(momentum)	$Kg^{-1/3}\, m^2\, sec^{-1}$
$K_R = \dot{\sigma}_{MAX}$	$m^{2/3}$	(rotor strength)	$Kg^{2/3}\, sec^{-1}$
$K_G = T_G$	$m^{-2/3}$	(gimbal torque)	$Kg^{1/3}\, m^2\, sec^{-2}$
$K_P = P_p$	$m^{-2/3}$	(dissipated power)	$Kg^{1/3}\, m^2\, sec^{-3}$

(54)

Other characteristics may be derived from these expressions, such as the spin rate $\Omega_s = h/J_s$, the maximum gimbal angular acceleration $\ddot{\sigma}_{MAX} = T_G/J$, or the output torque $T_V = h\dot{\sigma}_{MAX}^{\leftarrow}$:

$$\begin{cases} \Omega_s = K_H K_{J_s} m^{-1/3} \\ \ddot{\sigma}_{MAX} = K_G K_J m^{-1} \\ T_V = K_H K_R m^{2/3} \end{cases} \tag{55}$$

Table 3 gives the values, in SI units (see (54)), of the GSP's of a classical Sperry control moment gyro*, and of the smaller V-gyrodamper# used in the beam simulations of Section 2.

TABLE 3. SPERRY CMG AND GYRODAMPER SCALING PARAMETERS

	m	K_{J_s}	K_J	K_H	K_R	K_G	K_P
Sperry	78.75	673	861	2.0	36.7	.43	.87
Gyrodamper	8	1524	1524	.53	8	.8	2

The last five GSP's are directly related to the performance of the gyro control system: the larger they are, the better the performance. Once the design has maximized these parameters, then the mass m may be chosen to fit a particular application.

*Calculated from manufacturer's data (verbally transmitted).

#Calculated from Lockheed in-house preliminary design (see Fig. 4).

V-Gyrodampers Scaling Laws

The performance of the V-gyrodamper (gyro + feedback loop combination) will be now evaluated. The four conditions or limits described previously are first formulated in terms of the GSP using (54) and (55):

$$\begin{cases} 1) & |\sigma| \leq \sigma_{MAX} \\ 2) & |\dot{\sigma}| \leq K_R\, m^{-2/3} \\ 3) & |\ddot{\sigma}| \leq K_G K_J\, m^{-1} \\ 4) & P_p \leq K_p\, m^{2/3} \end{cases} \tag{56}$$

Then the relationship between the amplitudes of the local rotation angle θ (due to structural vibration) and the gimbal angle σ is obtained from the gyrodamper transfer function given in Eq. (45):

$$\frac{\sigma(\omega)}{\theta(\omega)} = \frac{i K' \omega}{\omega_G^2 - \omega^2 + i \omega_1 \omega} \tag{45}$$

Within the bandwidth of the system, this transfer function is essentially constant and the ratio of the amplitudes of σ and θ is then:

$$\sigma/\theta \cong K'/\omega_1$$

As was shown before, Eq. (47), this system acts as a rate-feedback controller since its torque output is

$$T_V = -D\dot{\theta}$$

where

$$D = 2hK'/\omega_1$$

Thus

$$\sigma/\theta = D/2h \tag{57}$$

Replacing in (56) $\begin{cases} |\dot{\sigma}| \text{ by } \sigma\omega \\ |\ddot{\sigma}| \text{ by } \sigma\omega^2 \\ P_p \text{ by } J\sigma^2\omega^3 \end{cases}$

and using (57) and (54), the conditions (56) become:

$$\begin{cases} \text{gimbal travel} & \theta \leq 2D^{-1}K_H m^{4/3}\sigma_{MAX} \\ \text{gimbal rate} & \theta \leq 2D^{-1}K_H K_R m^{2/3}\omega^{-1} \\ \text{gimbal acceleration} & \theta \leq 2D^{-1}K_H K_G K_J m^{1/3}\omega^{-2} \\ \text{power} & \theta \leq 2D^{-1}K_H K_p^{1/2} K_J^{1/2} m^{5/6}\omega^{-3/2} \end{cases} \tag{58}$$

This indicates that the magnitude of the initial vibration present in the structure (and reflected by the local rotation angle θ) that can be handled by the gyrodampers is bounded by four limits, three of which are frequency dependent as shown in Figure 13.

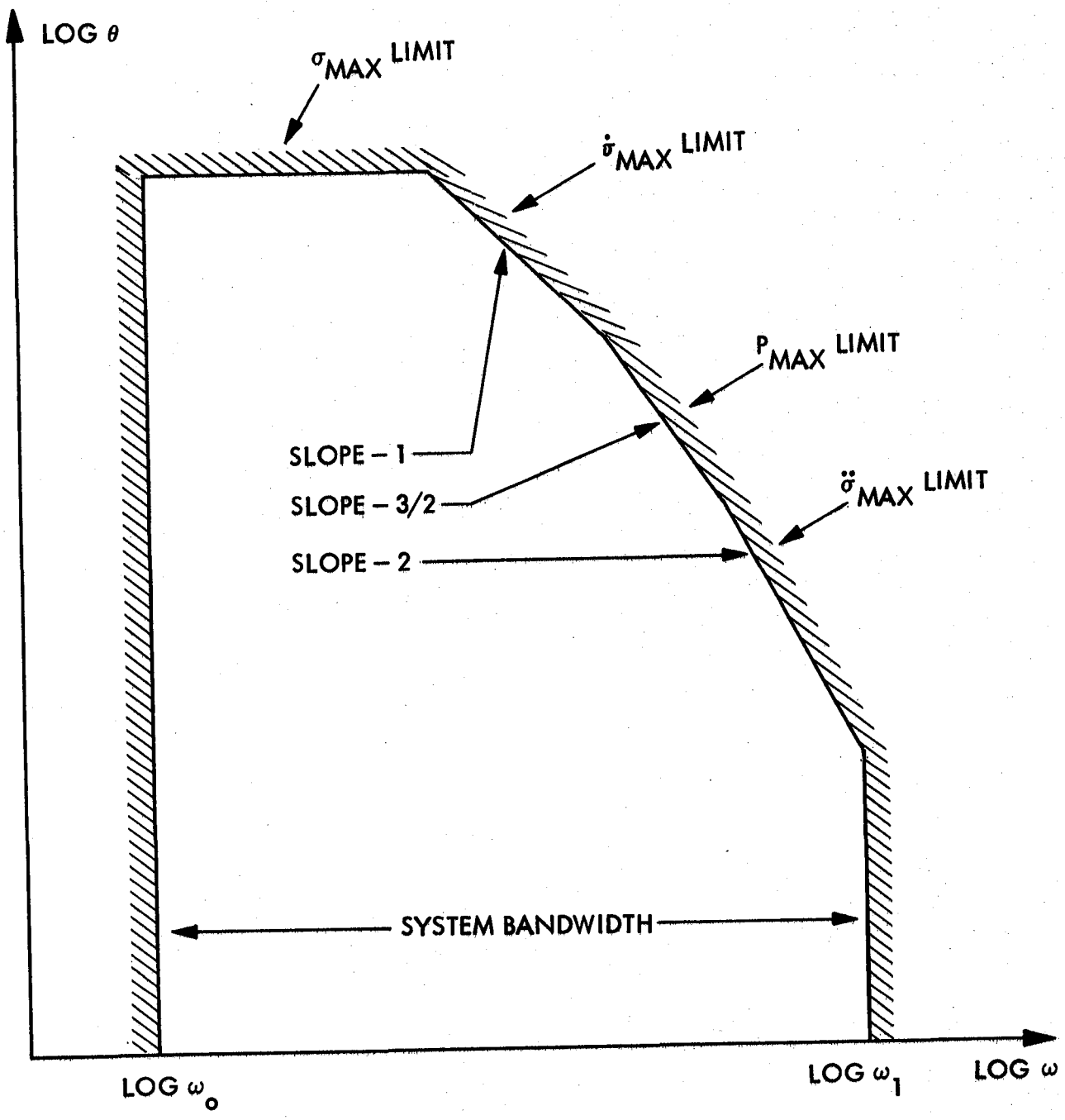

Figure 13. Typical region of operation of gyrodampers

More amplitude can be tolerated if the damping gain D is decreased, but then, because of the low authority controller formula (16), the damping ratio will also decrease. Conversely, if more damping is needed, D must be increased, but then less vibratory amplitude can be removed. The quantity $\zeta\theta$ appears therefore naturally as a better variable to express the conditions (58). Since ζ is not only related to D but also to the properties of the structure by Eq. (16), and because the structure will vibrate mainly at frequencies near its modal frequencies, some scaling parameters will first be derived for the structure itself.

Structure Scaling Parameters

Considering the case of a uniform beam damped about one axis by one V-gyrodamper (as was the case for the previous simulations), the generalized formula (35) leads to:

$$2\,\zeta_n\,\omega_n = D\,\phi_n'^2 \tag{59}$$

where ϕ_n' represents the nth "rotation mode shape" at the actuator (and sensor) location. (The indices a and r have been dropped to simplify the notation.) In this case

$$\phi_n'(x) = \frac{\partial \phi_n(x)}{\partial x} \tag{60}$$

where $\phi_n(x)$ is the usual deformation mode shape at a distance x from the origin of the beam. Assuming that the gyrodamper is at the origin of a free-free beam, classical beam theory shows that* (ref. 8):

$$\begin{cases} \phi_n'^2 \cong 4\beta_n^2 M^{-1} L^{-2} \\ \omega_n = \beta_n^2 M^{-1/2} L^{-3/2} (EI)^{1/2} \end{cases} \tag{61}$$

*In the reference, β_n and L are respectively called λ_n and ℓ.

where β_n is the dimensionless nth root of the frequency equation and depends only upon the boundary conditions, L is the beam length, M its total mass, I the cross-sectional inertia and E the Young's modulus. Defining:

$$K_s \equiv (EI)^{-1/2} \tag{62}$$

Eq. (59) may be expressed as:

$$\zeta_n = 2D\, K_s M^{-1/2} L^{-1/2} \tag{63}$$

Thus this particular structure can be characterized in terms of its length and mass, its bending stiffness parameter K_s and its dimensionless frequencies β_n.

V-Gyrodamped Structure Scaling Laws

Before assembling the formulas of Eqs. (58)–(63) for obtaining the scaling laws for the total system, two new parameters have to be introduced. First, for performance and reliability reasons, there will generally be more than one damper controlling a particular direction in the structure. Thus let N be the total number of V-gyrodampers. Second, a reasonable mass ratio should be considered between the damper system and the structure itself. Let μ be this ratio:

$$\mu \triangleq \frac{Nm}{M} \tag{64}$$

We note that with N dampers, the damping ratio will be N times greater; thus (63) becomes:

$$\zeta_n = 2DNK_s M^{-1/2} L^{-1/2} \tag{65}$$

Using (64) and (65) the following scaling laws are obtained from conditions (58):

$$
\begin{cases}
\sigma \text{ limit} & \zeta_n \theta_n \le 4\, N^{-1/3} K_H \sigma_{MAX} & \mu^{4/3} & K_s M^{5/6} L^{-1/2} \\
\dot{\sigma} \text{ limit} & \zeta_n \theta_n \le 4\, N^{1/3} K_H K_R & \mu^{2/3} & K_s M^{1/6} L^{-1/2} \omega_n^{-1} \\
\ddot{\sigma} \text{ limit} & \zeta_n \theta_n \le 4\, N^{2/3} K_H K_J K_G & \mu^{1/3} & K_s M^{-1/6} L^{-1/2} \omega_n^{-2} \\
P \text{ limit} & \zeta_n \theta_n \le \underbrace{4\, N^{1/6} K_H K_J^{1/2} K_P^{1/2}}_{\text{Gyro parameters}} & \underbrace{\mu^{5/6}}_{\substack{\text{Mass} \\ \text{ratio}}} & \underbrace{K_s M^{1/3} L^{-1/2} \omega_n^{-3/2}}_{\text{Structure parameters}}
\end{cases}
\tag{66}
$$

Here θ_n represents the angular vibration at the modal frequency ω_n and ζ_n the corresponding damping ratio introduced by the gyrodampers. These damping ratios are independent of the frequency as shown in (65) and this is a particular property resulting from using damping torques, which involve local rotation modes, and from locating the gyros at the extremities of the beam. If the gyros were situated differently, then Eq. (65) will be frequency dependent. For instance, at the center of the beam, $\zeta_n = 0$ for all the symmetric modes.

The conditions (66) may be plotted in the same way as displayed in Fig. 12, except that now the quantity $\zeta_n \theta_n$ is plotted instead of θ. Since the modal frequencies are related to the structure parameters by Eq. (61), it is possible to reformulate Eq. (66) as:

$$
\begin{cases}
\sigma \text{ limit} & \zeta_n \theta_n \le 4\, N^{-1/3} & K_H \sigma_{MAX} & \mu^{4/3} & K_s M^{5/6} L^{-1/2} & \\
\dot{\sigma} \text{ limit} & \zeta_n \theta_n \le 4\, N^{1/3} & K_H K_R & \mu^{2/3} & K_s^2 M^{2/3} L & \beta_n^{-2} \\
\ddot{\sigma} \text{ limit} & \zeta_n \theta_n \le 4\, N^{2/3} & K_H K_J K_G & \mu^{1/3} & K_s^3 M^{5/6} L^{5/2} & \beta_n^{-4} \\
P \text{ limit} & \zeta_n \theta_n \le \underbrace{4\, N^{1/6}}_{\text{Gyro parameters}} & \underbrace{K_H K_J^{1/2} K_P^{1/2}}_{\text{Gyro parameters}} & \underbrace{\mu^{5/6}}_{\substack{\text{Mass} \\ \text{ratio}}} & \underbrace{K_s^{5/2} M^{13/12} L^{7/4}}_{\text{Structure parameters}} & \beta_n^{-3}
\end{cases}
\tag{67}
$$

These scaling laws are valid for beams and beam-like structures. For instance, they could be applied to a rectangular platform and its bending modes controlled by gyrodampers situated along the edges or corners. There are of course many ways in which to use these laws. Some particular applications (see Figures 14 and 15) are shown below for the following values of the parameters:

K_H	K_R	K_G	K_J	K_P	K_s
2.5	23.4	1.03	800	2.05	$1.5\ 10^{-5}$

The above parameters correspond to the following CMG design: m = 8 kg, J = 0.04 kg-m^2, h = 40 Nm-sec, $\dot{\sigma}_{max}$ = 5.85 rad/sec, T_G = 4.12 Nm, P_p = 8 watts. The nominal structural design is chosen as μ = 0.1, M = 800 kg, L = 200 m, and the first two bending-mode roots are:

$$\beta_1 = 4.73 \quad , \quad \beta_2 = 7.93$$

Sometimes it is useful to use the parameter θ_n/τ_n, where τ_n is the decay time of the damped nth mode, instead of $\theta_n \zeta_n$, when mission requirements impose that the structure be quiet after a certain time. Since $\tau_n = 1/\zeta_n \omega_n$, formulas similar to (67) may be obtained by using Eq. (61) to eliminate ω_n. Figures 16 and 17 show the influence of the length L and of the number N of dampers or the parameter θ_n/τ_n. This last scaling is particularly interesting: it shows that, for damping purposes, it is more advantageous to use several little gyros than a large one. This is due to the fact that the performance is limited by the rotor strength ($\dot{\sigma}_{max}$) and the gimbal motor capability ($\ddot{\sigma}_{max}$). This is in contradistinction to the use of gyros for attitude control where the momentum capability (i.e., σ) or the power consumption may be dominant factors, in which case the curves of Figure 17 show that one unit is preferable to many. However, this last condition becomes important as N increases so that there is, in general, an optimum number of dampers for a given structure.

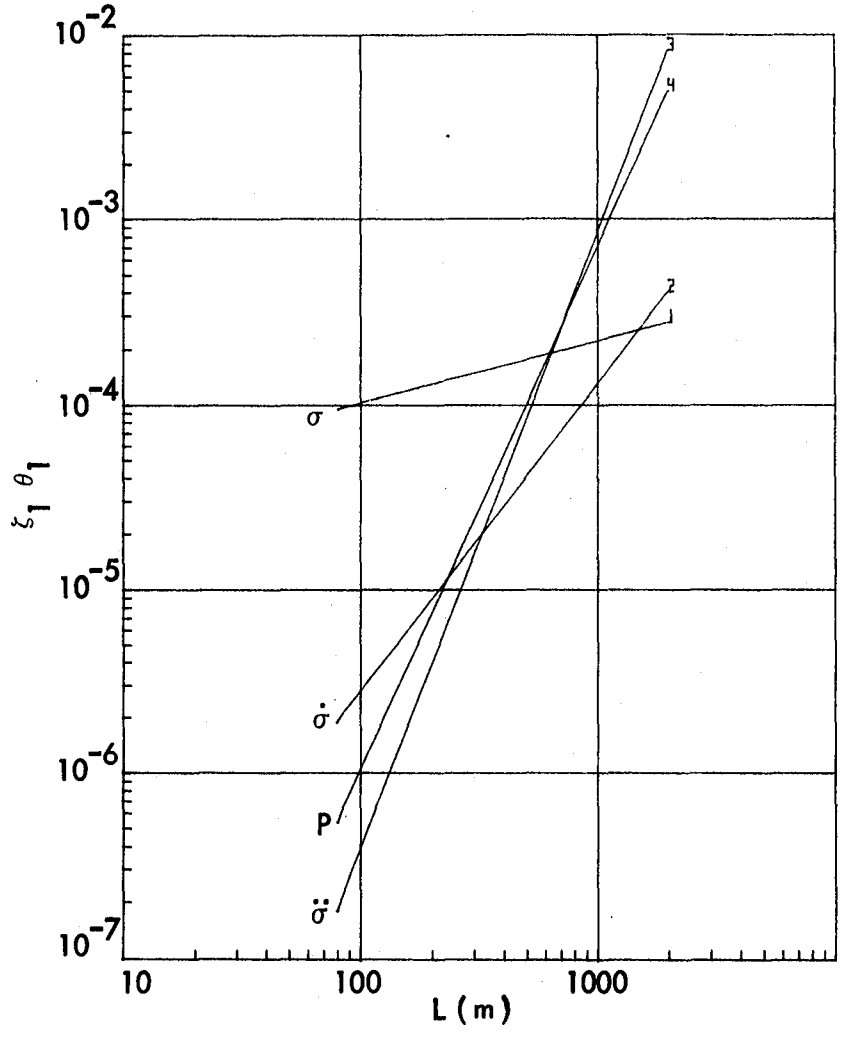

(1) STRUCTURE OF VARYING LENGTH ONLY
(M ~ L)

$$\zeta_n \theta_n \leq C_1 L^{1/3}$$

$$\zeta_n \theta_n \leq C_2 L^{5/3} \beta_n^{-2}$$

$$\zeta_n \theta_n \leq C_3 L^{10/3} \beta_n^{-4}$$

$$\zeta_n \theta_n \leq C_4 L^{17/6} \beta_n^{-3}$$

Figure 14. Particularized scaling laws – structure of varying length only

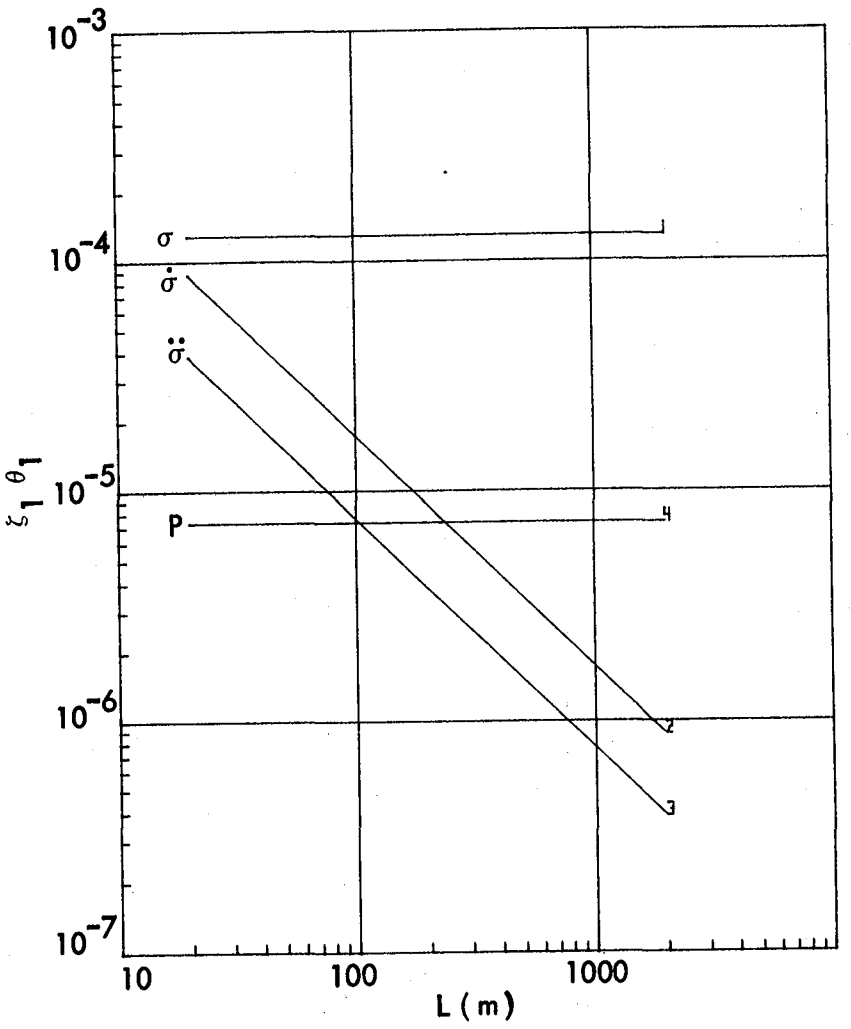

(2) HOMOTHETIC HOMOGENEOUS STRUCTURE (E = CONSTANT)
($M \sim L^3$, $K_s \sim L^{-2}$)

$$\zeta_n \theta_n \leq C_1'$$

$$\zeta_n \theta_n \leq C_2' L^{-1} \beta_n^{-2}$$

$$\zeta_n \theta_n \leq C_3' L^{-1} \beta_n^{-4}$$

$$\zeta_n \theta_n \leq C_4' \beta_n^{-3}$$

HO-MO-THET'IC, *adj.* **homothetic figures.** Figures so related that lines joining corresponding points pass through a point and are divided in a constant ratio by this point.

homothetic transformation. See SIMILITUDE—transformation of similitude.

(WHERE THE C's ARE CONSTANTS INDEPENDENT OF L)

Figure 15. Particularized scaling laws — homothetic homogeneous structure

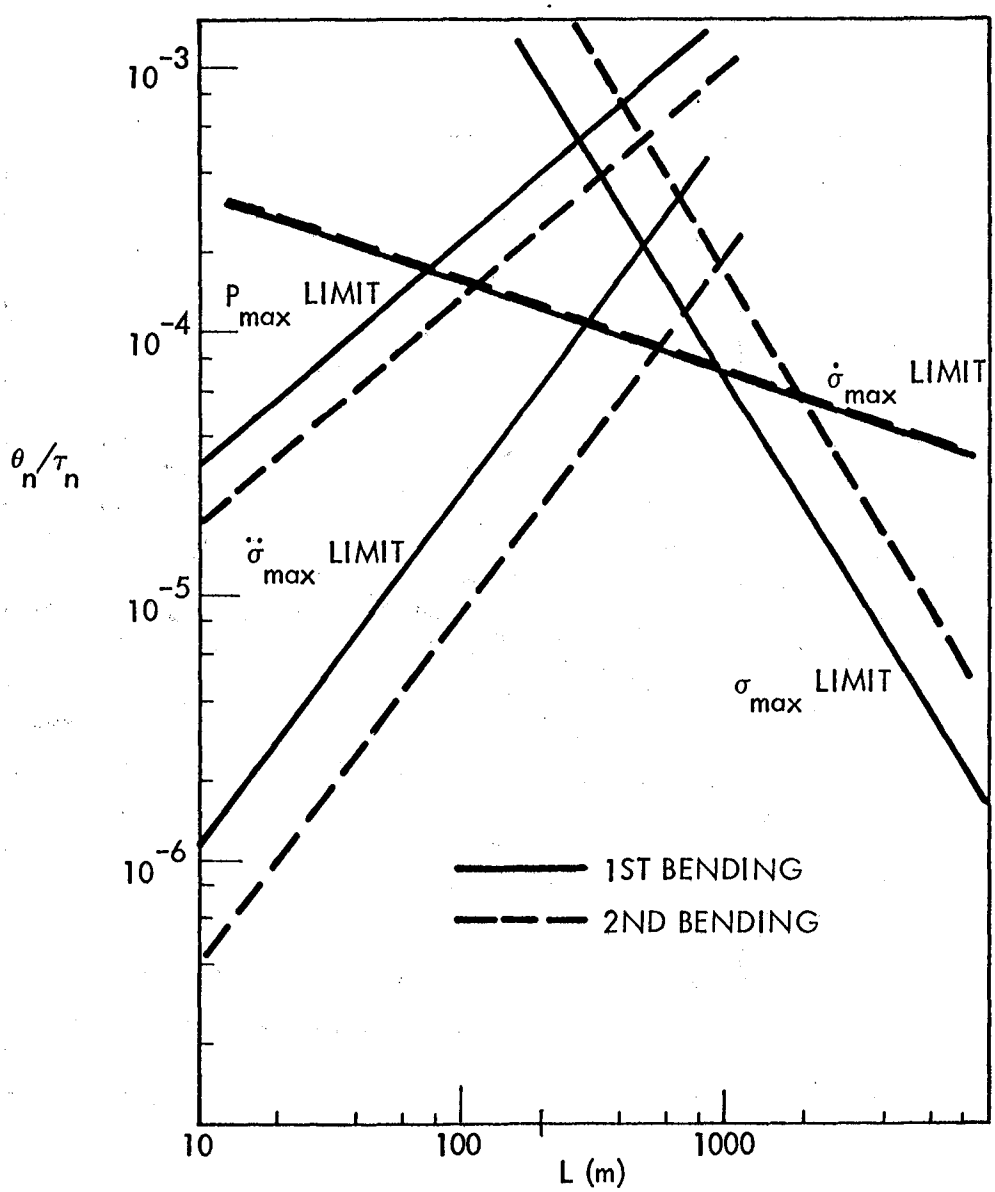

Figure 16. Gyrodamper performance versus structure length (Beam-like structure with gyrodampers at tips)

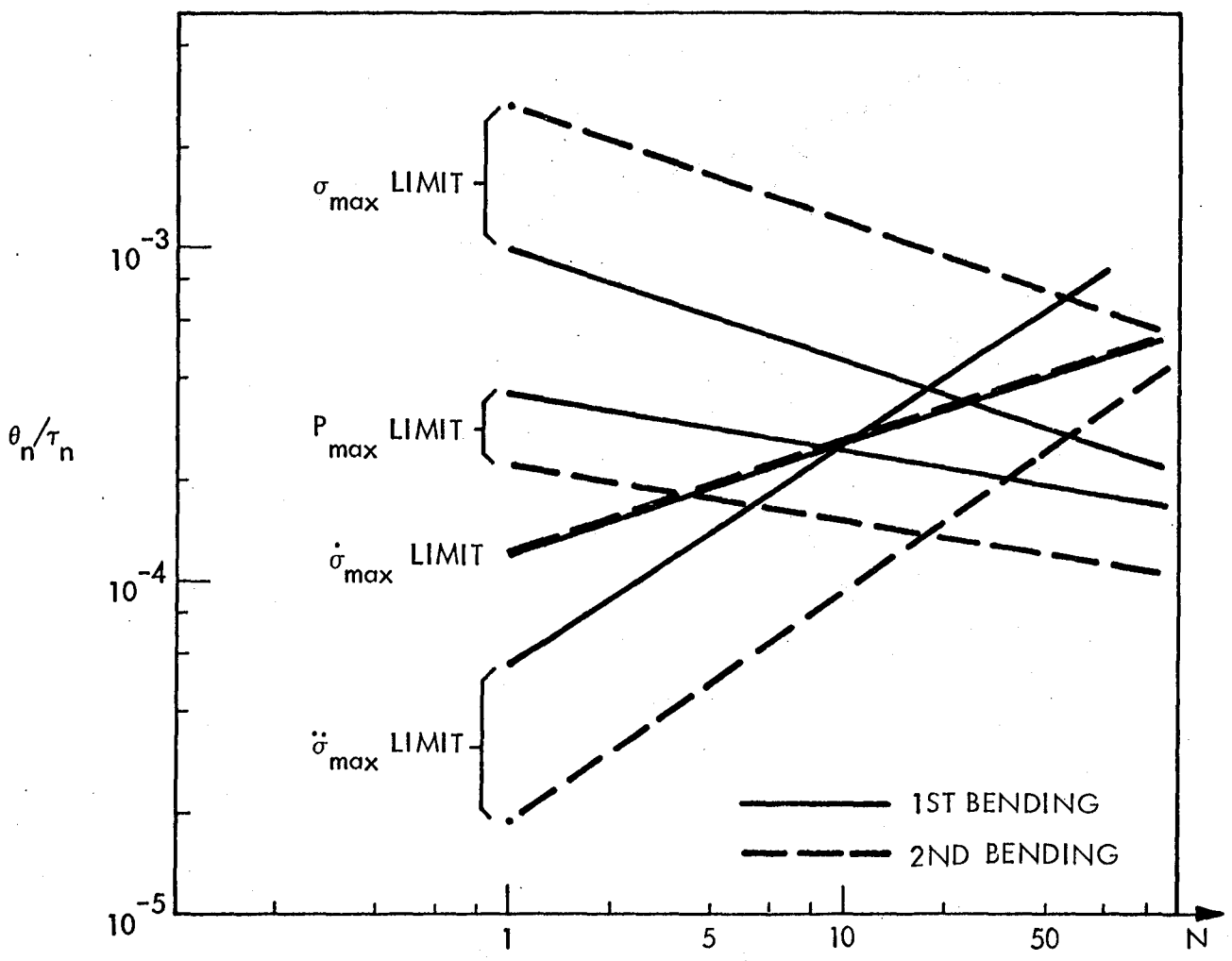

Figure 17. Gyrodamper performance versus number of units for constant mass ratio (Beam-like structure with gyrodampers at tips)

CONCLUSION AND RECOMMENDATION

The feasibility of controlling the vibrations of a structure by colocated sensor/actuator damping devices has been demonstrated in this study using beam or beam-like structures and gyrodampers as an example. Scaling laws have been derived using the Low Authority Structural Control theory and the physical properties of control moment gyros. These laws provide excellent tools for the design of low authority control systems for beams or beam-like structures and permit extrapolation of the results for structures of different characteristics.

The control of structural flexiblility implies, in some sense, the ability to construct, in space, large space strucutres whose behavior is determined predominantly not by passive characteristics but by active control systems. In this preliminary investigation, it was useful to direct consideration to a few simple models in the hope that generic characteristics of the control process will emerge and be directly applicable to more detailed, realistic systems. Experience with detailed structural models, however, has already indicated that system performance metrics, such as rms surface shape, rf or optical performance measures, modal damping, etc., can be extremely sensitive to changes in the structural model, actuator and sensor placement, and sensor measurement error. These sensitivities may also result from the detailed way a portion or all of the structure is built, the limitations of sensor measurement, or the disturbances associated with specific actuator implementations. Therefore, while consideration of quite simple structures is a necessary first step in obtaining knowledge of fundamentals, it should not generally be expected that control strategies developed in this way can be immediately implemented on real, high-detail structures. For the latter, questions of local versus global control, sensor/actuator placement strategy and error, model accuracy and identification, modal density, and computational requirements will be dominant considerations.

The positive results obtained in this study strongly motivate further investigations on more complicated structures, since the fundamental phenomena are now better understood. In particular, a rectangular reticulated space platform made of the 102-in. NASA graphite epoxy columns will provide a more generic example on which to evaluate both transient effects and external disturbances, while being controlled by gyrodampers.

Also an investigation into other kinds of damping devices is needed, in particular into the linear-inertial type ("proof mass" damper), so that tradeoff studies between various actuator types could be available.

Finally, the analytical and simulation results obtained in the present study will serve as a basis for design of a laboratory experiment which will attempt to demonstrate the practical implementation of structural control.

Appendix A

EQUATIONS OF MOTION FOR A BEAM CARRYING V-GYRO UNITS*

The differential equations governing the motion in an inertially fixed plane A of a beam B equipped with an arbitrary number of V-gyro units can be derived as follows: First, to put B into a general configuration in A, introduce A_1 and A_2 (see Fig. A-1a) as perpendicular lines fixed in A, intersecting at point O. Align the neutral axis ν of B with A_1 such that the intersection of ν with one end of B lies at O. Next, treating B as if it were rigid, move this point of B to a point Q of A (see Fig. A-1b). The position vector $\underline{p}^{Q/O}$ of Q relative to O is then given by

$$\underline{p}^{Q/O} = X\,\underline{a}_1 + Y\,\underline{a}_2 \tag{A.1}$$

where $\underline{a}_1$ and $\underline{a}_2$ are unit vectors parallel to A_1 and A_2 as shown. Now rotate B an amount θ relative to A_1, letting C_1 and C_2 be lines respectively parallel and perpendicular to ν and intersecting at Q. Finally, subject B to a flexural deformation relative to C_1 (see Fig. A-1c), so that the position vector $\underline{p}^{\tilde{P}/Q}$ from Q to a point $\tilde{P}$ of ν can be expressed as

$$\underline{p}^{\tilde{P}/Q} = x\,\underline{c}_1 + y\,\underline{c}_2 \tag{A.2}$$

where $\underline{c}_1$ and $\underline{c}_2$ are unit vectors respectively parallel to C_1 and C_2, as shown. A is presumed to be a principal plane of flexure for B.

---

*By David A. Levinson.

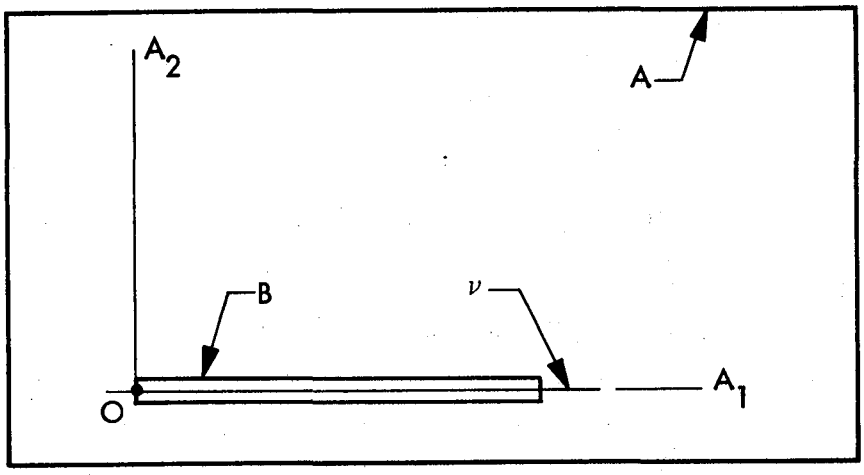

(a) Initial alignment

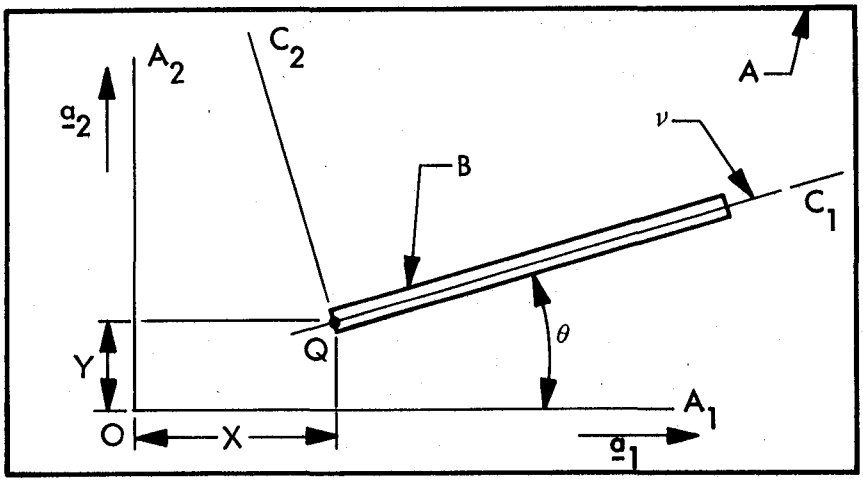

(b) Translation and rotation

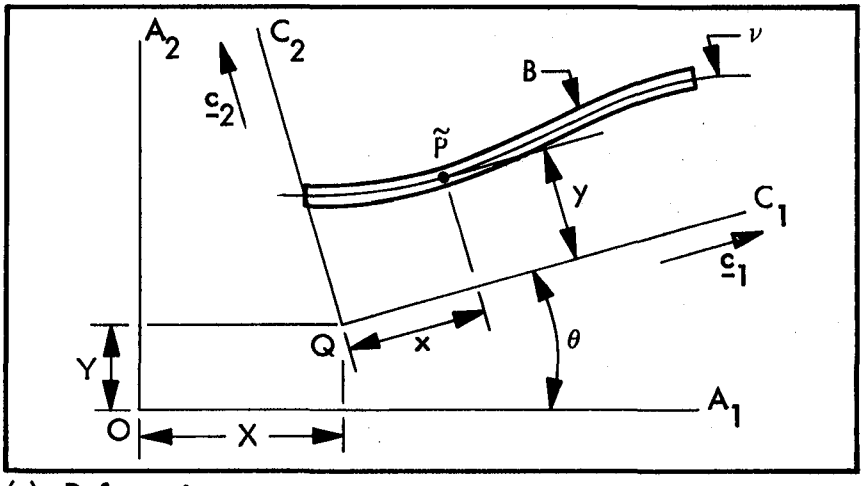

(c) Deformation

Figure A-1 General configuration of a beam in an inertially fixed plane

Next, it is assumed that y can be written

$$y = \sum_{i=1}^{n} q_i \phi_i \tag{A.3}$$

where $q_1, \ldots, q_n$ are functions of only the time t, and $\phi_1, \ldots, \phi_n$ depend only upon x. Defining the functions $U_1, \ldots, U_{3+n}$ as

$$U_1 \triangleq \dot{X} \cos\theta + \dot{Y} \sin\theta \tag{A.4}$$

$$U_2 \triangleq -\dot{X} \sin\theta + \dot{Y} \cos\theta \tag{A.5}$$

$$U_3 \triangleq \dot{\theta} \tag{A.6}$$

$$U_{3+i} \triangleq \dot{q}_i \qquad (i = 1, \ldots, n) \tag{A.7}$$

one then can express the velocity ${}^{A}\underline{v}^{\tilde{P}}$ and acceleration ${}^{A}\underline{a}^{\tilde{P}}$ of $\tilde{P}$ in A as

$${}^{A}\underline{v}^{\tilde{P}} = \left(U_1 - U_3 \sum_{i=1}^{n} q_i \phi_i\right) \underline{c}_1 + \left(U_2 + \sum_{i=1}^{n} U_{3+i} \phi_i + U_3 x\right) \underline{c}_2 \tag{A.8}$$

and

$${}^{A}\underline{a}^{\tilde{P}} = \left(\dot{U}_1 - \dot{U}_3 \sum_{i=1}^{n} q_i \phi_i - 2U_3 \sum_{i=1}^{n} U_{3+i} \phi_i - U_2 U_3 - U_3^2 x\right) \underline{c}_1$$
$$+ \left(\dot{U}_2 + \sum_{i=1}^{n} \dot{U}_{3+i} \phi_i + \dot{U}_3 x + U_3 U_1 - U_3^2 \sum_{i=1}^{n} q_i \phi_i\right) \underline{c}_2 \tag{A.9}$$

Partial velocities $\overset{A}{\underset{\sim}{v}}_{1}^{\tilde{P}}, \ldots, \overset{A}{\underset{\sim}{v}}_{3+n}^{\tilde{P}}$ associated respectively with $U_1, \ldots, U_{3+n}$ then can be determined from Eq. (A.8) and are found to be (Ref. 9, p. 26)

$$\overset{A}{\underset{\sim}{v}}_{1}^{\tilde{P}} = \underset{\sim}{c}_1 \tag{A.10}$$

$$\overset{A}{\underset{\sim}{v}}_{2}^{\tilde{P}} = \underset{\sim}{c}_2 \tag{A.11}$$

$$\overset{A}{\underset{\sim}{v}}_{3}^{\tilde{P}} = -\sum_{j=1}^{n} q_j \phi_j \underset{\sim}{c}_1 + x \underset{\sim}{c}_2 \tag{A.12}$$

$$\overset{A}{\underset{\sim}{v}}_{j+3}^{\tilde{P}} = \phi_j \underset{\sim}{c}_2 \tag{A.13}$$

Letting L and ρ stand for the length and the mass per unit length of B, one can form the contribution $\left(F_\ell^*\right)_B$ to the generalized inertia force associated with U_ℓ ($\ell = 1, \ldots, 3 + n$) from the relation (Ref. 9, p. 89)

$$\left(F_\ell^*\right)_B = -\int_0^L \overset{A}{\underset{\sim}{v}}_{\ell}^{\tilde{P}} \cdot \overset{A}{\underset{\sim}{a}}^{\tilde{P}} \rho \, dx \tag{A.14}$$

Equations (A.9) through (A.14) give

$$\left(F_1^*\right)_B = -\dot{U}_1 M + \dot{U}_3 \sum_{i=1}^{n} q_i \Phi_i + 2U_3 \sum_{i=1}^{n} U_{3+i} \Phi_i + U_2 U_3 M + U_3^2 d \tag{A.15}$$

$$\left(F_2^*\right)_B = - \dot{U}_2 M - \sum_{i=1}^{n} \dot{U}_{3+i} \Phi_i - \dot{U}_3 d - U_3 U_1 M + U_3^2 \sum_{i=1}^{n} q_i \Phi_i \qquad (A.16)$$

$$\left(F_3^*\right)_B = \dot{U}_1 \sum_{i=1}^{n} q_i \Phi_i - \dot{U}_3 \sum_{i=1}^{n} \sum_{j=1}^{n} q_i q_j E_{ij} - 2U_3 \sum_{i=1}^{n} \sum_{j=1}^{n} q_i U_{3+j} E_{ij}$$

$$- U_2 U_3 \sum_{i=1}^{n} q_i \Phi_i - \dot{U}_2 d - \sum_{i=1}^{n} \dot{U}_{3+i} N_i - \dot{U}_3 I - U_3 U_1 d \qquad (A.17)$$

$$\left(F_{3+j}^*\right)_B = - \dot{U}_2 \Phi_j - \sum_{i=1}^{n} \dot{U}_{3+i} E_{ij} - \dot{U}_3 N_j - U_3 U_1 \Phi_j$$

$$+ U_3^2 \sum_{i=1}^{n} q_i E_{ij} \qquad (j = 1, \ldots, n) \qquad (A.18)$$

where

$$M \triangleq \int_0^L \rho \, dx \qquad (A.19)$$

$$d \triangleq \int_0^L x \rho \, dx \qquad (A.20)$$

$$I \triangleq \int_0^L x^2 \rho \, dx \qquad (A.21)$$

$$\Phi_i \triangleq \int_0^L \phi_i \rho \, dx \qquad (i = 1, \ldots, n) \qquad (A.22)$$

$$N_i \triangleq \int_0^L x\,\phi_i\,\rho\,dx \qquad (i = 1, \ldots, n) \tag{A.23}$$

$$E_{ij} \triangleq \int_0^L \phi_i\,\phi_j\,\rho\,dx \qquad (i, j = 1, \ldots, n) \tag{A.24}$$

If one chooses for ϕ_i $(i = 1, \ldots, n)$ the so-called free-free modes of a uniform beam, that is (Ref. 8),

$$\phi_i \triangleq M^{-1/2}\{\cosh(\lambda_i x/L) + \cos(\lambda_i x/L) - R_i[\sinh(\lambda_i x/L) + \sin(\lambda_i x/L)]\}$$
$$(i = 1, \ldots, n) \tag{A.25}$$

where $\lambda_1, \ldots, \lambda_n$ are consecutive roots of the equation

$$\cos\lambda \cosh\lambda - 1 = 0 \tag{A.26}$$

and

$$R_i \triangleq (\cosh\lambda_i - \cos\lambda_i)/(\sinh\lambda_i - \sin\lambda_i) \qquad (i = 1, \ldots, n) \tag{A.27}$$

then, with ρ = constant, the integrals in Eqs. (A.19) through (A.24) become

$$M = \rho L \tag{A.28}$$

$$d = \rho L^2/2 = ML/2 \tag{A.29}$$

$$I = \rho L^3/3 = ML^2/3 \tag{A.30}$$

$$\Phi_i = 0 \qquad (i = 1, \ldots, n) \tag{A.31}$$

$$N_i = 0 \qquad (i = 1, \ldots, n) \tag{A.32}$$

$$E_{ij} = \delta_{ij} \qquad (i, j = 1, \ldots, n) \tag{A.33}$$

where δ_{ij} is the Kronecker delta.

Equations (A.15) through (A.18) thus give way to

$$\left(F_1^*\right)_B = - \dot{U}_1 M + U_2 U_3 M + U_3^2 d \tag{A.34}$$

$$\left(F_2^*\right)_B = - \dot{U}_2 M - \dot{U}_3 d - U_3 U_1 M \tag{A.35}$$

$$\left(F_3^*\right)_B = - \dot{U}_3 \left(I + \sum_{i=1}^{n} q_i^2\right) - \dot{U}_2 d - U_3 U_1 d - 2U_3 \sum_{i=1}^{n} q_i U_{3+i} \tag{A.36}$$

$$\left(F_{3+j}^*\right)_B = - \sum_{i=1}^{n} \dot{U}_{3+j} + U_3^2 q_j \qquad (j = 1, \ldots, n) \tag{A.37}$$

Mounted on B are n_G V-gyro units $V1, \ldots, Vn_G$, a typical one of which, $V\alpha$, is shown in Fig. A-2. The arrangement consists of a gyro casing $G\alpha$ attached to B, and two identical uniform rotors, $D\alpha$ and $E\alpha$, carried by gimbals whose axes lie in A, are parallel to each other, and are "perpendicular" to ν in the following sense: the mass center of $G\alpha$ and of each rotor-gimbal assembly are presumed to remain in A, with the mass center $P\alpha$ of $V\alpha$ being a point fixed on ν; thus, if $\underline{b}_{1\alpha}$ and $\underline{b}_{2\alpha}$ are unit vectors parallel to A and respectively parallel and perpendicular to ν at $P\alpha$, then the gimbal axes are parallel to $\underline{b}_{2\alpha}$.

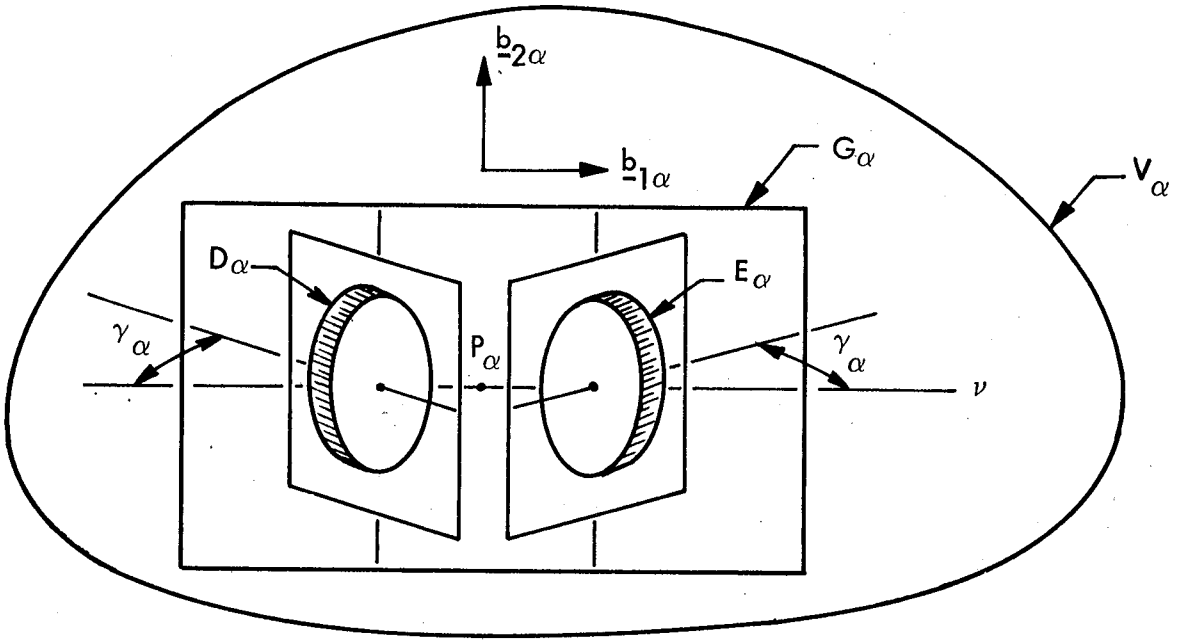

Figure A-2 V-gyro unit

The gimbals are geared to each other in such a way that the axes of $D\alpha$ and $E\alpha$ each rotate the same amount γ_α relative to ν, but in opposite senses, as shown. $D\alpha$ and $E\alpha$ are made to rotate with a constant angular speed Ω_α relative to their respective gimbals such that when $\gamma_\alpha = 0$, the angular velocities of $D\alpha$ and $E\alpha$ in $G\alpha$ are $-\Omega_\alpha \underline{b}_{1\alpha}$ and $\Omega_\alpha \underline{b}_{1\alpha}$, respectively.

If C denotes the reference frame in which C_1 and C_2 are fixed, then the angular velocity ${}^{C}\underline{\omega}^{G\alpha}$ of $G\alpha$ in C can be expressed as

$$ {}^{C}\underline{\omega}^{G\alpha} = \frac{\partial}{\partial t}\left(\frac{\partial y}{\partial x}\right)\Big|_{x_\alpha} \underline{c}_3 \qquad (\alpha = 1, \ldots, n_G) \tag{A.38} $$

where $\underline{c}_3 \triangleq \underline{c}_1 \times \underline{c}_2$, and $(\partial y/\partial x)|_{x_\alpha}$ is the value of $\partial y/\partial x$ evaluated at $x = x_\alpha$, the x-coordinate of $P\alpha$. Substitution from Eq. (A.3) into Eq. (A.38) and comparison with Eq. (A.7) then gives

$$ {}^{C}\underline{\omega}^{G\alpha} = \sum_{i=1}^{n_G} U_{3+i}\,(d\phi_i/dx)\Big|_{x_\alpha} \underline{c}_3 \qquad (\alpha = 1, \ldots, n_G) \tag{A.39} $$

where $(d\phi_i/dx)|_{x_\alpha}$ is the value of $d\phi_i/dx$ at $x = x_\alpha$. Then, noting that the angular velocities ${}^{G\alpha}\underline{\omega}^{D\alpha}$, ${}^{G\alpha}\underline{\omega}^{E\alpha}$ of $D\alpha$ and $E\alpha$ in $G\alpha$ and the angular velocity ${}^{A}\underline{\omega}^{C}$ of C in A are given by

$$ {}^{G\alpha}\underline{\omega}^{D\alpha} = -\Omega_\alpha \cos\gamma_\alpha \underline{b}_{1\alpha} - U_{3+n+\alpha}\,\underline{b}_{2\alpha} - \Omega_\alpha \sin\gamma_\alpha \underline{c}_3 \qquad (\alpha = 1, \ldots, n_G) \tag{A.40} $$

$$G\alpha_{\underline{\omega}}E\alpha = \Omega_\alpha \cos\gamma_\alpha \, \underline{b}_{1\alpha} + U_{3+n+\alpha} \, \underline{b}_{2\alpha} - \Omega_\alpha \sin\gamma_\alpha \, \underline{c}_3 \qquad (\alpha = 1, \ldots, n_G) \tag{A.41}$$

$$A_{\underline{\omega}}C = U_3 \, \underline{c}_3 \tag{A.42}$$

where

$$U_{3+n+\alpha} \triangleq \dot{\gamma}_\alpha \qquad (\alpha = 1, \ldots, n_G) \tag{A.43}$$

one can form the angular velocities $A_{\underline{\omega}}D\alpha$, $A_{\underline{\omega}}E\alpha$ of $D\alpha$ and $E\alpha$ in A by using Eqs. (A.39) through (A.42) and the addition theorem for angular velocities (Ref. 9, p. 24), obtaining the expressions

$$A_{\underline{\omega}}D\alpha = -\Omega_\alpha \cos\gamma_\alpha \, \underline{b}_{1\alpha} - U_{3+n+\alpha} \, \underline{b}_{2\alpha} + \left[U_3 + \sum_{i=1}^{n} U_{3+i} \left(d\phi_i/dx\right)\Big|_{x_\alpha} - \Omega_\alpha \sin\gamma_\alpha \right] \underline{c}_3 \qquad (\alpha = 1, \ldots, n_G) \tag{A.44}$$

$$A_{\underline{\omega}}E\alpha = \Omega_\alpha \cos\gamma_\alpha \, \underline{b}_{1\alpha} + U_{3+n+\alpha} \, \underline{b}_{2\alpha} + \left[U_3 + \sum_{i=1}^{n} U_{3+i} \left(d\phi_i/dx\right)\Big|_{x_\alpha} - \Omega_\alpha \sin\gamma_\alpha \right] \underline{c}_3 \qquad (\alpha = 1, \ldots, n_G) \tag{A.45}$$

Differentiating Eqs. (A.44), (A.45) with respect to t in A then yields the angular accelerations ${}^{A}\underline{\xi}D\alpha$ and ${}^{A}\underline{\xi}E\alpha$ of $D\alpha$ and $E\alpha$ in A,

$$
\begin{aligned}
{}^{A}\underline{\xi}D\alpha = & \left[\Omega_\alpha U_{3+n+\alpha} \sin\gamma_\alpha + U_3 U_{3+n+\alpha} + \sum_{i=1}^{n} U_{3+i} (d\phi_i/dx)\big|_{x_\alpha} U_{3+n+\alpha}\right] \underline{b}_{1\alpha} \\
& - \left[\dot{U}_{3+n+\alpha} + U_3 \Omega_\alpha \cos\gamma_\alpha + \sum_{i=1}^{n} U_{3+i} (d\phi_i/dx)\big|_{x_\alpha} \Omega_\alpha \cos\gamma_\alpha\right] \underline{b}_{2\alpha} \\
& + \left[\dot{U}_3 + \sum_{i=1}^{n} \dot{U}_{3+i} (d\phi/dx)\big|_{x_\alpha} - \Omega_\alpha U_{3+n+\alpha} \cos\gamma_\alpha\right] \underline{c}_3 \\
& (\alpha = 1, \ldots, n_G) \qquad \text{(A.46)}
\end{aligned}
$$

$$
\begin{aligned}
{}^{A}\underline{\xi}E\alpha = & -\left[\Omega_\alpha U_{3+n+\alpha} \sin\gamma_\alpha + U_3 U_{3+n+\alpha} + \sum_{i=1}^{n} U_{3+i} (d\phi_i/dx)\big|_{x_\alpha} U_{3+n+\alpha}\right] \underline{b}_{1\alpha} \\
& + \left[\dot{U}_{3+n+\alpha} + U_3 \Omega_\alpha \cos\gamma_\alpha + \sum_{i=1}^{n} U_{3+i} (d\phi_i/dx)\big|_{x_\alpha} \Omega_\alpha \cos\gamma_\alpha\right] \underline{b}_{2\alpha} \\
& + \left[\dot{U}_3 + \sum_{i=1}^{n} \dot{U}_{3+i} (d\phi_i/dx)\big|_{x_\alpha} - \Omega_\alpha U_{3+n+\alpha} \cos\gamma_\alpha\right] \underline{c}_3 \quad (\alpha = 1, \ldots, n_G) \\
& \qquad \text{(A.47)}
\end{aligned}
$$

Furthermore, Eqs. (A.44), (A.45) provide partial angular velocities ${}^{A}\underline{\omega}_{\ell}D\alpha$, ${}^{A}\underline{\omega}_{\ell}E\alpha$ associated with U_ℓ ($\ell = 1, \ldots, 3 + n + n_G$), these being given by (Ref. 9, p. 17)

$$
\left.
\begin{aligned}
&{}^{A}\underline{\omega}^{D\alpha}_{1} = {}^{A}\underline{\omega}^{D\alpha}_{2} = {}^{A}\underline{\omega}^{E\alpha}_{1} = {}^{A}\underline{\omega}^{E\alpha}_{2} = 0 \\
&{}^{A}\underline{\omega}^{D\alpha}_{3} = {}^{A}\underline{\omega}^{E\alpha}_{3} = \underline{c}_3 \\
&{}^{A}\underline{\omega}^{D\alpha}_{3+j} = {}^{A}\underline{\omega}^{E\alpha}_{3+j} = (d\phi_j/dx)\big|_{x_\alpha}\,\underline{c}_3 \qquad (j=1, \ldots, n) \\
&{}^{A}\underline{\omega}^{D\alpha}_{3+n+\alpha} = -\,{}^{A}\underline{\omega}^{E\alpha}_{3+n+\alpha} = \underline{b}_{2\alpha}
\end{aligned}
\right\} (\alpha = 1, \ldots, n_G)
\tag{A.48}
$$

and, if one assumes that the central inertia ellipsoid of each rotor-gimbal assembly is a sphere with associated moment of inertia J_α, then the inertia torques $(\underline{T}^*)_{D\alpha}$, $(\underline{T}^*)_{E\alpha}$ acting respectively on $D\alpha$ and $E\alpha$ are given by (Ref. 9, p. 116)

$$
(\underline{T}^*)_{D\alpha} = -\,J_\alpha\,{}^{A}\underline{\xi}^{D\alpha} \qquad (\alpha = 1, \ldots, n_G) \tag{A.49}
$$

$$
(\underline{T}^*)_{E\alpha} = -\,J_\alpha\,{}^{A}\underline{\xi}^{E\alpha} \qquad (\alpha = 1, \ldots, n_G) \tag{A.50}
$$

The acceleration ${}^{A}\underline{a}^{P\alpha}$ and partial velocities ${}^{A}\underline{v}^{P\alpha}_{\ell}$ $(\ell = 1, \ldots, 3 + n + \alpha)$ of $P\alpha$ in A can be written [see Eqs. (A.8), (A.9)]

$$\underline{A}_{P\alpha} = \left(\dot{U}_1 - \dot{U}_3 \sum_{i=1}^{n} q_i \phi_i|_{x_\alpha} - 2U_3 \sum_{i=1}^{n} U_{3+i} \phi_i|_{x_\alpha} - U_2 U_3 - U_3^2 x_\alpha \right) \underline{c}_1$$

$$+ \left(\dot{U}_2 + \sum_{i=1}^{n} \dot{U}_{3+i} \phi_i|_{x_\alpha} + \dot{U}_3 x_\alpha + U_3 U_1 - U_3^2 \sum_{i=1}^{n} q_i \phi_i|_{x_\alpha} \right) \underline{c}_2 \tag{A.51}$$

$$\underline{A}_{\underline{v}_1 P\alpha} = \underline{c}_1 \tag{A.52}$$

$$\underline{A}_{\underline{v}_2 P\alpha} = \underline{c}_2 \tag{A.53}$$

$$\underline{A}_{\underline{v}_3 P\alpha} = - \sum_{j=1}^{n} q_j \phi_j|_{x_\alpha} \underline{c}_1 + x_\alpha \underline{c}_2 \qquad (\alpha = 1, \ldots, n_G) \tag{A.54}$$

$$\underline{A}_{\underline{v}_{3+j} P\alpha} = \phi_j|_{x_\alpha} \underline{c}_2 \qquad (j = 1, \ldots, n) \tag{A.55}$$

$$\underline{A}_{\underline{v}_{3+n+\alpha} P\alpha} = 0 \qquad (\alpha = 1, \ldots, n_G) \tag{A.56}$$

where $\phi_i|_{x_\alpha}$ denotes the value of ϕ_i at $x = x_\alpha$ $(\alpha = 1, \ldots, n_G)$.

Finally, if m_α is the mass of $V\alpha$, and if one assumes that the distance between the centers of $D\alpha$ and $E\alpha$ is small compared with L $(\alpha = 1, \ldots, n_G)$, then the contribution $(F_\ell^*)_V$ from $V1, \ldots, Vn_G$ to the generalized inertia force associated with U_ℓ $(\ell = 1, \ldots, 3 + n + n_G)$ is given by (Ref. 9, p. 123)

$$\left(F_{\ell}^{*}\right)_{V} = \sum_{\alpha=1}^{n_G} \left[{}^{A}\underline{\omega}_{\ell}^{D\alpha} \cdot \left(\underline{T}^{*}\right)_{D\alpha} + {}^{A}\underline{\omega}_{\ell}^{E\alpha} \cdot \left(\underline{T}^{*}\right)_{E\alpha} - m_{\alpha}\, {}^{A}\underline{v}_{\ell}^{P\alpha} \cdot \underline{a}^{P\alpha} \right]$$

$$(\ell = 1, \ldots, 3 + n + n_G) \qquad \text{(A.57)}$$

Substitution from Eqs. (A.46) through (A.56) into Eq. (A.57) then produces

$$\left(F_{1}^{*}\right)_{V} = - \sum_{\alpha=1}^{n_G} m_{\alpha} \left(\dot{U}_1 - \dot{U}_3 \sum_{i=1}^{n} q_i \phi_i \big|_{x_\alpha} - 2U_3 \sum_{i=1}^{n} U_{3+i} \phi_i \big|_{x_\alpha} - U_2 U_3 - U_3^2 x_{\alpha} \right)$$

(A.58)

$$\left(F_{2}^{*}\right)_{V} = - \sum_{\alpha=1}^{n_G} m_{\alpha} \left(\dot{U}_2 + \sum_{i=1}^{n} \dot{U}_{3+i} \phi_i \big|_{x_\alpha} + \dot{U}_3 x_{\alpha} + U_3 U_1 - U_3^2 \sum_{i=1}^{n} q_i \phi_i \big|_{x_\alpha} \right)$$

(A.59)

$$\begin{aligned}\left(F_{3}^{*}\right)_{V} = - \sum_{\alpha=1}^{n_G} m_{\alpha} \Bigg[& - \sum_{j=1}^{n} q_j \phi_j \big|_{x_\alpha} \left(\dot{U}_1 - \dot{U}_3 \sum_{i=1}^{n} q_i \phi_i \big|_{x_\alpha} - 2U_3 \sum_{i=1}^{n} U_{3+i} \phi_i \big|_{x_\alpha} \right. \\ & \left. - U_2 U_3 + x_{\alpha} \left(\dot{U}_2 + \sum_{i=1}^{n} \dot{U}_{3+i} \phi_i \big|_{x_\alpha} + \dot{U}_3 x_{\alpha} + U_3 U_1 \right) \right) \Bigg] \\ & - 2 \sum_{\alpha=1}^{n_G} \left\{ J_{\alpha} \left[\dot{U}_3 + \sum_{i=1}^{n} \dot{U}_{3+i} \left(d\phi_i / dx \right) \big|_{x_\alpha} - \Omega_{\alpha} U_{3+n+\alpha} \cos \gamma_{\alpha} \right] \right\}\end{aligned}$$

(A.60)

$$\left(F^*_{3+j}\right)_V = -\sum_{\alpha=1}^{n_G} m_\alpha \phi_j|_{x_\alpha}\left(\dot{U}_2 + \sum_{i=1}^{n} \dot{U}_{3+i}\,\phi_i|_{x_\alpha} + \dot{U}_3\, x_\alpha + U_3\, U_1 - U_3^2 \sum_{i=1}^{n} q_i\,\phi_i|_{x_\alpha}\right) - 2\sum_{\alpha=1}^{n_G}\left\{J_\alpha\,(d\phi_i/dx)|_{x_\alpha}\left[\dot{U}_3 + \sum_{i=1}^{n} \dot{U}_{3+i}\,(d\phi_i/dx)|_{x_\alpha} - \Omega_\alpha\, U_{3+n+\alpha}\cos\gamma_\alpha\right]\right\}$$

$$(j = 1, \ldots, n) \qquad \text{(A.61)}$$

$$\left(F^*_{3+n+\alpha}\right)_V = -2J_\alpha\left[\dot{U}_{3+n+\alpha} + U_3\,\Omega_\alpha\cos\gamma_\alpha + \sum_{i=1}^{n} U_{3+i}\,(d\phi_i/dx)|_{x_\alpha}\,\Omega_\alpha\cos\gamma_\alpha\right]$$

$$(\alpha = 1, \ldots, n_G)$$

(A.62)

It is further assumed that the inertia torques acting on $G\alpha$ ($\alpha = 1, \ldots, n_G$) are small in comparison with the inertia torques given by Eqs. (A.49), (A.50), and, hence, are neglected in this analysis.

Motors attached to $G\alpha$ exert systems of forces on the gimbals carrying $D\alpha$ and $E\alpha$ equivalent to couples of torques $\underline{T}_\alpha$ and $-\underline{T}_\alpha$, respectively, where

$$\underline{T}_\alpha = T_\alpha\,\underline{b}_{2\alpha} \qquad (\alpha = 1, \ldots, n_G) \qquad \text{(A.63)}$$

Thus, the generalized active force $F_{3+n+\alpha}$ associated with $U_{3+n+\alpha}$ ($\alpha = 1, \ldots, n_G$) can be obtained from the expression (Ref. 9, p. 81)

$$F_{3+n+\alpha} = \sum_{\alpha=1}^{n_G} \left({}^{A}\underline{\omega}^{D\alpha}_{3+n+\alpha} \cdot \underline{T}_{\alpha} - {}^{A}\underline{\omega}^{E\alpha}_{3+n+\alpha} \cdot \underline{T}_{\alpha} \right) \quad (\alpha = 1, \ldots, n_G) \quad (A.64)$$

and is found from Eq. (A.63) and the last of Eq. (A.48) to be

$$F_{3+n+\alpha} = -2\, T_{\alpha} \qquad (\alpha = 1, \ldots, n_G) \qquad (A.65)$$

The generalized active forces associated with internal forces in B can be found from a strain energy function S and a dissipation function D, given by

$$S \triangleq (1/2) \int_0^L EI\, (\partial^2 y/\partial x^2)^2\, dx \qquad (A.66)$$

and

$$D \triangleq (1/2) \int_0^L c\, (\partial y/\partial t)^2\, dx \qquad (A.67)$$

where the flexural rigidity EI of B and the structural damping coefficient c of B are constants. Substitution from Eq. (A.3) into Eqs. (A.66), (A.67) then gives

$$S = (1/2) \sum_{i=1}^{n} \sum_{j=1}^{n} s_{ij}\, q_i\, q_j \qquad (A.68)$$

and

$$D = (1/2) \sum_{i=1}^{n} \sum_{j=1}^{n} d_{ij}\, \dot{q}_i\, \dot{q}_j \qquad (A.69)$$

where

$$s_{ij} \triangleq EI \int_0^L (d^2 \phi_i/dx^2)\, (d^2 \phi_j/dx^2)\, dx \qquad (i,j = 1,\ldots,n) \qquad (A.70$$

$$d_{ij} \triangleq c \int_0^L \phi_i\, \phi_j\, dx \qquad (i,j = 1,\ldots,n) \qquad A.71)$$

Evaluation of the integrals in Eqs. (A.70), (A.71), by reference to Eq. (A.25), produces the relations

$$s_{ij} = EI\ \lambda_i^4\ \delta_{ij}/(ML^3) \qquad (i,j = 1,\ldots,n) \qquad (A.72)$$

$$d_{ij} = c\ L\ \delta_{ij}/M \qquad (i,j = 1,\ldots,n) \qquad (A.73)$$

so that one has, from Eqs. (A.68), A.69), and (A.7),

$$S = (1/2) \sum_{i=1}^{n} \omega_i^2\ q_i^2 \qquad (A.74)$$

$$D = [c\,L/(2M)] \sum_{i=1}^{n} U_{3+i}^2 \qquad (A.75)$$

where

$$\omega_i^2 = EI\ \lambda_i^4/(ML^3) \quad (i = 1,\ldots,n) \qquad (A.76)$$

Finally, the generalized active force F_{3+j} associated with U_{3+j} $(j = 1,\ldots,n)$ can be obtained from the expression

$$F_{3+j} = -\partial S/\partial q_j - \partial D/\partial U_{3+j} \qquad (j = 1,\ldots,n) \qquad (A.77)$$

which leads to

$$F_{3+j} = -\omega_j^2\ q_j - c\,U_{3+j} \qquad (j = 1,\ldots,n) \qquad (A.78)$$

The $3+n+n_G$ dynamical equations governing the (force-free) motion of the system can now be constructed as follows* (Ref. 9, p. 177):

$$\left(F_1^*\right)_B + \left(F_1^*\right)_V = 0 \qquad \text{(A.79)}$$

(A.34) (A.58)

$$\left(F_2^*\right)_B + \left(F_2^*\right)_V = 0 \qquad \text{(A.80)}$$

(A.35) (A.59)

$$\left(F_3^*\right)_B + \left(F_3^*\right)_V = 0 \qquad \text{(A.81)}$$

(A.36) (A.60)

$$\left(F_{3+j}^*\right)_B + \left(F_{3+j}^*\right)_V + F_{3+j} = 0 \quad (j = 1, \ldots, n) \qquad \text{(A.82)}$$

(A.37) (A.61) (A.78)

$$\left(F_{3+n+\alpha}^*\right)_V + F_{3+n+\alpha} = 0 \quad (\alpha = 1, \ldots, n_G) \qquad \text{(A.83)}$$

(A.62) (A.65)

A complete description of the motion of the system can be obtained from Eqs. (A.79) through (A.83) together with the kinematical equations, Eqs. (A.4) through (A.7), (A.43), once initial values of X, Y, θ, $q_1, \ldots, q_n$, $\gamma_1, \ldots, \gamma_{n_G}$, $U_1, \ldots, U_{3+n+n_G}$ have been provided.

*Numbers in parentheses beneath terms refer to correspondingly numbered equations.

Appendix B
LOCAL ROTATION MODES

In the earlier discussion of Generalized Modes and Force Distributions, reference was made, for three-dimensional structures, to "local rotation" mode shapes obtained by "stacking" the three-dimensional curls $\vec{\nabla} \times \vec{\phi}_n$ of the deformation mode shapes. This concept is a direct application of a kinematical theorem due to Helmholtz who establishes the following well-known result at the beginning of his paper on vortex motions (ref. 10): The most general motion of a sufficiently small element of a deformable body can be represented as the composition of

1. a translation
2. a rotation
3. an extension (contraction) in three mutually orthogonal directions

The proof is based on the multiple Taylor expansion of the relative displacement of two neighboring points in terms of their original coordinate differences. In the context of linear elastic structures, we will restrict ourselves to differential displacements, ignoring the constant term giving rise to translation.

We consider 3-d.o.f. finite-element structures in which a point located at $\vec{r}$ undergoes a deformation which displaces it to $\vec{r} + \vec{u}$, as shown in Figure B-1. The deformation $\vec{u}$ is a time-varying vector field $\vec{u} = \vec{u}(\vec{r}, t)$, and for finite-element structures, is modally decomposed in a set of (usually) orthogonal functions $\{ \vec{\phi}_n \}$:

$$\vec{u}(\vec{r}, t) = \sum_n q_n(t)\, \vec{\phi}_n(\vec{r}) \qquad \text{(B.1)}$$

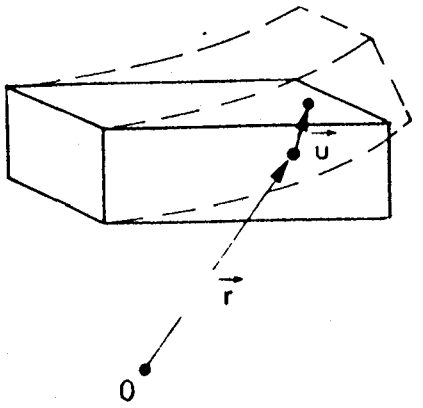

Figure B-1. Local structural deformation

where $q_n(t)$ are the modal amplitudes associated with the decomposition in the mode shape basis $\{\vec{\phi}_n\}$.

The differential deformation between two points situated at $\vec{r}$ and $\vec{r} + d\vec{r}$ before the deformation is then given by

$$d\vec{u} = (\vec{\nabla}\vec{u}) \cdot d\vec{r} \tag{B.2}$$

where $\vec{\nabla}\vec{u}$ is the tensor spatial gradient of the deformation field $\vec{u}(\vec{r}, t)$. This tensor may be split into its symmetric and skew-symmetric parts (using Gibbs' dyadic notation):

$$\vec{\nabla}\vec{u} = \underbrace{\frac{1}{2}(\vec{\nabla}\vec{u} + \vec{u}\vec{\nabla})}_{\mathcal{S}\ :\ \text{Strain Tensor (Symmetric)}} + \underbrace{\frac{1}{2}(\vec{\nabla}\vec{u} - \vec{u}\vec{\nabla})}_{\frac{1}{2}(\vec{\nabla}\vec{u} \times \vec{u}) \times \mathbf{1}\ \text{(Skew-Symmetric)}} \tag{B.3}$$

where $\mathbf{1}$ is the identity dyadic. If we define:

$$\vec{\delta\theta} \equiv \frac{1}{2}\left(\vec{\nabla} \times \vec{u}\right) \tag{B.4}$$

the differential deformation Eq. (B.2) can be written as

$$\left.\begin{aligned} d\vec{u} &= \left(\mathcal{S} + \vec{\delta\theta} \times 1\right) \cdot d\vec{r} \\ &= \mathcal{S} \cdot d\vec{r} + \vec{\delta\theta} \times d\vec{r} \end{aligned}\right\} \tag{B.5}$$

and $\vec{\delta\theta} = \vec{\delta\theta}\left(\vec{r}, t\right)$ is thus the instantaneous axis of rotation of a local material neighborhood of a point of the structure.

To obtain the "local rotation" modes, we substitute Eq. (B.1) into Eq. (B.4) to obtain

$$\left.\begin{aligned} \vec{\delta\theta} = \frac{1}{2}\left(\vec{\nabla} \times \vec{u}\right) &= \sum_n q_n(t)\left[\frac{1}{2}\left(\vec{\nabla} \times \vec{\phi}_n\right)\right] \\ &= \sum_n \vec{q}_n(t)\,\vec{\delta\theta}_n(\vec{r}) \end{aligned}\right\} \tag{B.6}$$

where

$$\vec{\delta\theta}_n(\vec{r}) \equiv \frac{1}{2}\left(\vec{\nabla} \times \vec{\phi}_n\right) \tag{B.7}$$

is the nth modal rotation coefficient, i.e., the contribution of the nth mode to the local instantaneous axis of rotation at a point $\vec{r}$. The corresponding nth column of the local rotation modal matrix is then obtained by "stacking" columnwise the three components of the Gibbs vector $\vec{\delta\theta}_n$ according to the nodal sequence of structural stations employed in the finite-element decomposition initially used for the $\vec{\phi}_n$'s.

MODAL TILT COEFFICIENTS FOR SEGMENTS DEFINED BY n POINTS

A special case of the modal rotation coefficients occurs for flat, plate-like structures for which the instantaneous local rotation axis remains essentially tangent to the structure. This arises, for instance, when high-frequency shearing modes are ignored in a given structural model. This situation, in itself, does not justify a special formula simply because $\vec{\delta\theta}_n = \frac{1}{2}(\vec{\nabla} \times \vec{\phi}_n)$ now only has two nonzero components in the local frame. If, however, for a structure of this kind, several relatively well separated structural nodal points are attached to a rigid plate (supporting, for example, a set of gyrodampers), then the "small neighborhood" assumption required for Helmholtz's theorem is no longer valid.

To associate a local rotation (or tilt) axis with a finite rigid plate interconnecting a number of n distinct structural nodal points, one can, of course, resort to 6-d.o.f. finite-element models. The difficulty with this procedure comes from the numerical methodology employed in synthesizing (or "compressing") model data into the multibody nonlinear dynamics codes, which incorporate flexibility with the usual 3-d.o.f. finite-element models. A very good approximation can be obtained, for 3-d.o.f. finite element models, by assuming that the local deformation will move the rigid plate into an orientation which is assumed to coincide with the least squares best-fit plane for the n nodal points, deforming individually without the constraint of being bolted to a rigid plate.

The algorithm for this procedure is displayed in Figure B-2, and numerical comparisons with 6-d.o.f. finite-element models have established the validity of the procedure for the special "flat" structures considered.

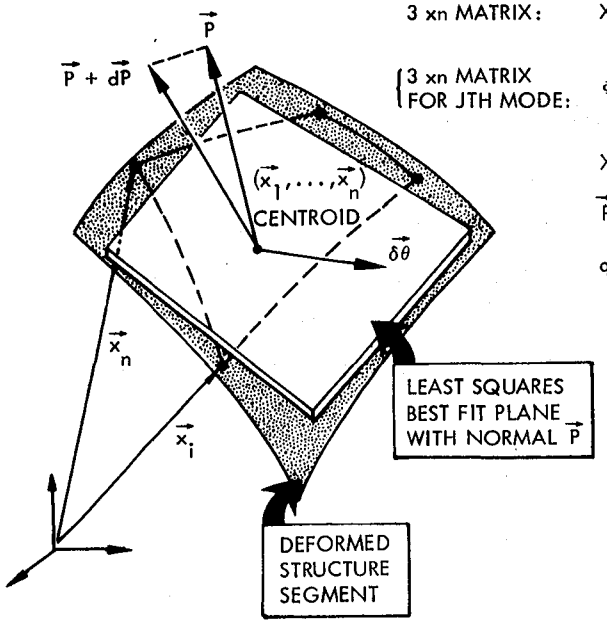

3 xn MATRIX: $X \equiv \left[\vec{x}_1, \ldots, \vec{x}_n\right]$ (n POINTS OF DEFORMED STRUCTURE)

{3 xn MATRIX FOR JTH MODE: $\Phi_j \equiv \left[\vec{\varphi}_j^1, \ldots, \vec{\varphi}_j^n\right]$ (JTH MODAL MATRIX AT THOSE n POINTS)

$X^\dagger \equiv (XX^T)^{-1} X$ (PSEUDOINVERSE OF X , 3 xn)

$\vec{P} = X^\dagger [1.1, \ldots, 1]^T$

$q_j(t)$: AMPLITUDE OF JTH MODE

- TILT DEFINED BY:

$$\delta\vec{\theta} \cong \frac{\vec{P} \times d\vec{P}}{|\vec{P}|^2} = -\frac{\vec{P}}{|\vec{P}|^2} \times \left[X^+ [dX]^T \vec{P}\right]$$

WHERE DEFORMATIONS $[dX] = \sum_j q_j(t) \left[\Phi_j\right]$

- DEFINE "MODAL TILT COEFFICIENTS" $\delta\vec{\theta}_j$ BY

$$\delta\vec{\theta}_j \equiv -\frac{\vec{P}}{|\vec{P}|^2} \times \left[X^\dagger \left(\Phi_j\right)^T \vec{P}\right] \text{ FOR JTH MODE}$$

SO THAT TOTAL TILT IS GIVEN BY:

$$\boxed{\delta\vec{\theta}(t) = \sum_j q_j(t)\, \delta\vec{\theta}_j}$$

Figure B-2. Modal tilt coefficients for segments defined by n points.

Appendix C
GYRODAMPER SCALING EXAMPLE

The following example illustrates the methodology for scaling a structural control system using gyrodampers. It is assumed that the structure is given, and that an existing CMG device, with acceptable performance, needs to be scaled to match the structure. In this instance, the structure is chosen to be a free-free aluminum beam with the following characteristics:

$$M = 154.6 \text{ kg}$$
$$L = 6.9 \text{ m}$$
$$I = 4.375\ 10^{-6} \text{ m}^4$$
$$E = 7.2\ 10^{10} \text{ Pa}$$
$$\rho = 2760 \text{ kg/m}^3$$
$$(K_s = (EI)^{-1/2} = 1.782\ 10^{-3})$$

The V-gyrodamper(s) will be located at one (both) ends of the beam. The scaling procedure is as follows:

Step 1. The values of the rotational mode shapes at the beam-ends are computed for the first few modes of interest (either analytically or by finite-element models). In this case, the first rotational mode shape is $\varphi_1 = 0.1098 \text{ rad kg}^{-1/2} \text{ m}^{-1}$ with a frequency $f_1 = 8.8$ Hz.

Step 2. The damping gain D is calculated from the desired damping ratio ζ using formula (16). In this case, a 10% damping ratio is desired in the first mode, leading to a gain

$$D = \frac{2\ \zeta_1\ \omega_1}{\varphi_1^2} = 916.55 \text{ Nms}$$

A full complex eigenanalysis of the system provides then then damping of the various modes. If not satisfactory, D is modified accordingly.

Step 3. An existing gyro design is selected. In this case, the CMG chosen is the Bendix Model No. MA5-100-1 shown in Table C-1 below. Its characteristics are:

$$
\begin{aligned}
m &= 17.3 \text{ kg} \\
h &= 6.78 \text{ Nms} \\
\Omega &= 8000 \text{ rpm} \\
J &= 0.01 \text{ kg m}^2 \\
\dot{\sigma}_{max} &= 20 \text{ rad/sec} \\
T_G &= 16.3 \text{ Nm} \\
P_p &= 320 \text{ watts}
\end{aligned}
$$

From Eq. (54), the following GSP are computed for this class of designs:

$$
\left.
\begin{aligned}
K_H &= 0.059 \\
K_R &= 214 \\
K_J &= 37,450 \\
K_G &= 1.523 \\
K_P &= 29.91
\end{aligned}
\right\} \text{ GSP Values}
$$

Step 4. The mass ratio μ is chosen on the basis of an acceptable weight for the control system, e.g., $\mu = 0.1$. Since $\mu \triangleq \frac{Nm}{M}$ from Eq. (64), the number N of V-CMG pairs can be increased provided smaller gyros are used such that the product Nm remains constant. The best value for N is determined then by examining the four limits given by Eq. (67). The corresponding composite graph of these inequalities is shown in Figure C-1, where the maximum vibration amplitude θ_1 is plotted versus the number N on a log-log scale. As can be seen in this particular example, the optimum choice is N = 2 V-CMG pairs.

Table C-1
BENDIX CONTROL MOMENT GYROS

MODEL NO:	MA-1000	MA-2300	MA-500 AC	MA-500 DC	MA-2000	MA-5-100-1
TYPE	DOUBLE GIMBAL	DOUBLE GIMBAL	SINGLE GIMBAL	SINGLE GIMBAL	DOUBLE GIMBAL	SINGLE GIMBAL
PROGRAM	CMG R and D	Skylab	CMG Test	CMG R and D	ADV. CMG	Pointer Control
AGENCY	NASA LRC	NASA MSFC	Air Force	In-House	NASA MSFC	LMSC
UNITS BUILT	4	12	3	5	1	5
STATUS	Evaluation at NASA	Qualified	Partially Qualified	Partially Qualified	Evaluation at NASA	Evaluation at LMSC
MOMENTUM (ft-lb-sec)	1000	2300	250 - 750	250 - 750	1000 - 3000	5
OUTPUT TORQUE Max ft-lb	175	122	500	500	175	100
PIVOT TORQUE Max ft-lb	175	122	90	90	175	12
DECREES OF FREEDOM	2	2	1	1	2	1
GIMBAL FREEDOM (deg)	Unlimited – Slip Rings	$\pm 80^\circ$ $\pm 175^\circ$	$\pm 170^\circ$	$\pm 170^\circ$	Unlimited – Slip Rings	Unlimited – Slip Rings
GIMBAL RATE Max (deg/sec)	10	4, 7	57.3	57.3	5, 30	1146
WEIGHT (lbs)	230	418	145	155	558	38
APPROX. ENVELOPE	39" Diam. Sphere	41" Diam. Sphere	(Cylinder 20" Diam. x 32" Long)		44" Diam. Sphere	Cylinder 10" x 10" Long
ROTOR SPEED (RPM)	11,400	9,000	7,850	7,850	4,000 to 12,000	8,000
SPIN UP TIME (hrs)	<4 hours	<14 hours	<6 hours	<2.5 hours	<2.5 hours (to 8,000 RPM)	<0.1

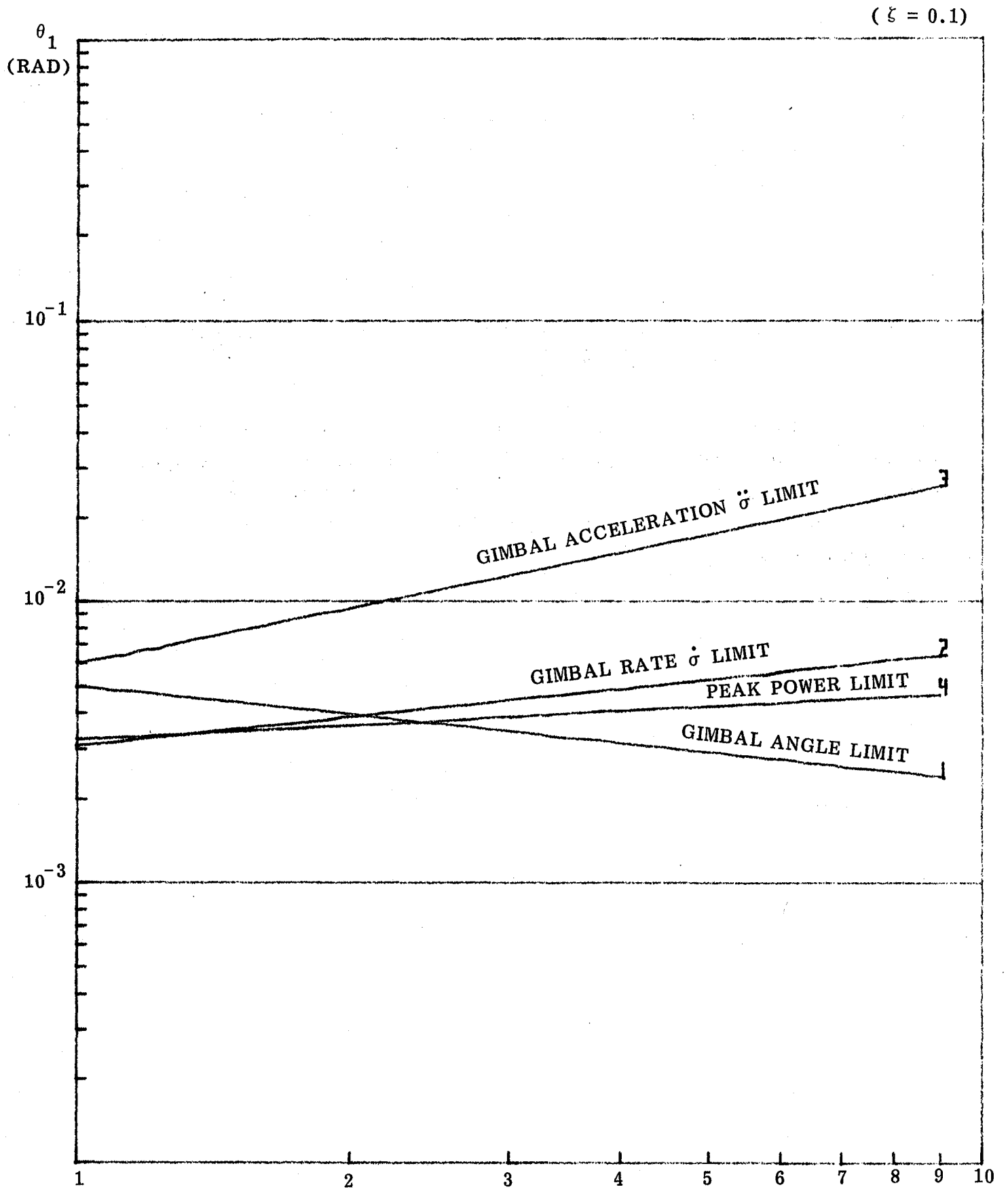

Figure C-1. Gyrodamper scaling example

Step 5. The characteristics of the required V-gyros are then obtained from their individual mass, i.e.,

$$m = \frac{\mu M}{N}$$

$$= 7.73 \text{ kg}$$

which is used in Eq. (54) with the GSP values given above. The geometric reduction factor is then $\sqrt[3]{7.73/17.3} = 0.764$.

Step 6. If the desired θ_1 is not high enough, the ratio μ can be increased (which will push all the limits upward). Otherwise, by examining the graph, manufacturer design modifications can be sought in order to meet desired performance. Eq. (67) could be used at that point to determine parametrically which gyro characteristics need to be improved.

REFERENCES

1. J. N. Aubrun, "Theory of the Control of Structures by Low Authority Controllers," AIAA Conference of Large Space Platforms: Future Needs and Capabilities, Los Angeles, Calif., 27–29 Sep 1978, Paper No. 78-1689

2. C. G. J. Hacobi, Crelles's Journal für die Reine und Angewandte Mathematik, Vol. 30, Berlin: de Gruyter, 1846, pp. 51–95

3. J. S. Przemieniecky, Theory of Matrix Structural Analysis, McGraw Hill, New York, 1968, p. 316

4. G. Margulies, J. N. Aubrun, D. Bushnell, and J. Y. L. Ho, "Multibody Flexible Spacecraft Integrated Analysis: Structures, Dynamics, and Control," AAS/AIAA Astrodynamics Conference, Wyoming, 7–9 Sep 1977

5. "Passive and Active Suppression of Vibration Response in Precision Structures, State-of-the-Art Assessment," Technical Report R 1138, Vol. 2, Technical Analysis, The Charles Stark Draper Laboratory, Inc., Cambridge, Mass., 28 Feb 1978. [Vol. 1 (S); Vol 2 (U)]

6. G. E. Fleischer, "Multibody System Applications and Simulations at the Jet Propulsion Laboratory," Dynamics of Multibody Systems, Ed. by K. Magnus, Springer-Verlag, Berlin Heidelberg New York, 1978, pp. 36–47

7. G. Margulies and J. N. Aubrun, "Geometric Theory of Single-Gimbal Control Moment Gyro Systems," J. Astronautical Sci., Vol. XXVI, No. 2, April-June 1978, pp. 159–191

8. W. Flügge, Handbook of Engineering Mechanics, New York, McGraw-Hill Book Company, Inc., 1962, pp. 61–8, 61–9

9. T. R. Kane, Dynamics, Stanford University, 1973

10. Helmholtz, H. v., "Über Integrale der hydrodynamischen Gleichungen, welche den Wirbelbewegungen entsprechen," Crelles J., 55, 25, 1858

REFERENCES (Cont.)

11. E. D. Scott, "Control Moment Gyro Gravity Stabilization," Progress in Astronautics and Aeronautics, Vol, 13, N.Y. Academic Press Inc., 1964, pp. 103-130.

12. E. D. Scott and J. J. Rodden, "Performance of Gravity-Gradient V-CMG Systems," AIAA Guidance, Control, and Flight Mechanics Conf., Princeton, N.J., AIAA Paper No. 69-831, Aug. 1969.